Genomic-Thermodynamic Phase Synchronization: Maxwell's Demon-Like Regulation of Cell Fate Transition

Masa Tsuchiya[1]*, Kenichi Yoshikawa[2] and Alessandro Giuliani[3]

[1]SEIKO Life Science Laboratory, SEIKO Research Institute for Education, Osaka, Japan
[2]Faculty of Life and Medical Sciences, Doshisha University, Kyotanabe, Japan
[3]Environment and Health Department, Istituto Superiore di Sanitá (Italian NIH), Rome, Italy

Conflict of Interest: The authors declare no conflict of interest.

*Correspondence: tsuchiya.masa@gmail.com

Abstract

Dynamic criticality - the balance between order and chaos - is fundamental in genome regulation and cellular transitions. In this study, we investigate the distinct behaviors of gene expression dynamics in MCF-7 breast cancer cells under two stimuli: Heregulin (HRG), which promotes cell fate transitions, and Epidermal Growth Factor (EGF), which, despite binding to the same receptor, does not induce cell fate changes. We model the system as an open, non-equilibrium thermodynamic system and introduce a convergence-based approach for the robust estimation of information-thermodynamic metrics.

Our analysis reveals that the Shannon entropy of the critical point (CP) dynamically synchronizes with the entropy of the rest of the whole expression system (WES), reflecting coordinated transitions between ordered and disordered phases. This phase synchronization is driven by net mutual information scaling with CP entropy dynamics, demonstrating how the CP governs genome-wide coherence. Notably, high-order (multivariate) mutual information emerges as a defining feature of the synergistic network underlying gene expression regulation.

By achieving thermodynamic phase synchronization, the CP orchestrates the entire expression system. Under HRG stimulation, the CP becomes active, functioning as a Maxwell's demon with dynamic, rewritable chromatin memory to guide a critical transition in cell fate. In contrast, during EGF stimulation, the CP remains inactive in this strategic role, acting passively to facilitate non-critical transition.

These findings establish a biophysical framework for cell fate determination, paving the way for innovative approaches in cancer research and stem cell therapy.

Introduction

Dynamic criticality in gene expression—characterized by shifts in global expression profiles initiated by changes in specific gene subsets—plays a pivotal role in regulating genome dynamics and driving critical transitions [Liu et al., 2017]. The delicate balance between order and chaos enables genomic regulation that is both flexible and stable [Zimatore et al. 2021; Shmulevich et al., 2005]

Our previous studies [Tsuchiya et al., 2014, 2015, 2016, 2020, 2022, 2023a, 2023b; Giuliani et al., 2017; Zimatore et al., 2021] demonstrated that this balance underpins both precise cellular responses to external signals and key processes such as cell differentiation and embryonic development. These dynamics are central to understanding cell fate changes. Our key findings are summarized below:

1. **Emergent self-organization within genome attractor**
   Self-organized critical (SOC) control of genome expression is governed by a key metric parameter, the Normalized Root Mean Square Fluctuation (*nrmsf*), which identifies distinct response domains (called critical states). Large groups of genes exhibit Coherent Stochastic Behavior (CSB), reducing noise and converging around centers of mass (CM), where each gene expression unit is treated as having unit mass [Tsuchiya et al., 2014, 2015]. These CMs function as attractors: the entire-genome CM is referred to as the Genome Attractor (GA), while local critical states act as super-critical or sub-critical attractors. Cyclic expression fluxes between these attractors constitute an open thermodynamic "genome engine" that regulates gene expression [Tsuchiya et al., 2020, 2022].
2. **CP as a central organizing hub**: A specific critical set of genes, referred to as the Critical Point (CP), exhibits bimodal singular behaviors according to the *nrmsf* metric. The CP functions as a central organizing hub, spreading high variability across the genome and driving critical transitions. When the system is pushed away from homeostasis, the state change at the CP propagates local perturbations across the genome, exemplifying SOC in the regulation of genomic expression [Tsuchiya et al., 2023a].
3. **Application CSB for modeling the genome engine through genomic stochastic thermodynamics**: The genome engine is modeled simply as a one-dimensional system,

where the expression level of a center of mass (CM) at a specific time point (x_t) represents "position," its first difference ($\Delta x_t = x_{t+1} - x_t$) reflects "momentum," and the second difference ($\Delta^2 x_t$) acts as "effective force" influencing changes in the system's energy (see more in [Tsuchiya et al., 2023b]). This model illustrates how the genome interacts dynamically with its environment, maintaining a nearly balanced influx and outflux over time. This balance demonstrates that the genome operates as an open stochastic thermodynamic system, aligning with insights from stochastic thermodynamics research (see review papers : [Parrondo et al., 2015; Ito, 2018; Peliti and Pigolotti, 2021; Shiraishi, 2023; Korbel and Wolpert, 2024]).

4. **Switching of cyclic flow in the genome engine at critical transitions:**
   Critical transitions in the genome engine lead to the reversal of cyclic expression fluxes [Tsuchiya et al., 2020, 2022]. These transitions are linked to structural changes, such as the bursting of peri-centromeric domains (PADs) in MCF-7 cancer cells, which impact the chromatin folding status [Krigerts et al., 2021], thereby enabling dynamic genomic regulation. By leveraging stochastic thermodynamics, this framework provides insights into how genomic regulation evolves over time, bridging molecular activities with broader structural and functional transformations.
5. **OMG–CP–GA network regulating sychronization of CP with GA for cell-fate change:**
   The OMG–CP–GA network governs cell-fate transitions by coordinating interactions among Oscillating-Mode Genes (OMG), identified by their high score on the second principal component (PC2), corresponding to the main direction of displacement from the GA [Zimatore et al. 2021], the Critical Point (CP), and the GA. OMG, often linked to the activation stages of signaling, modulate the synchronization between the CP and GA [Tsuchiya et al., 2023a]. This synchronization maintains genome-wide balance while enabling critical transitions. These transitions initiate genome-wide changes, leading to synchronized shifs in gene expression and chromatin remodeling. Rooted in the principles of self-organized criticality (SOC), this network provides a foundational genome engine mechanism for understanding how activated signals and critical transitions shape genomic dynamics and determine cell fate.

6. **Advancements over Classical Self-Organized Criticality Models**
   Synchronization between the CP and GA drives a "genome avalanche," spreading gene expression changes across WES. Unlike classical Self-Organized Criticality (c-SOC) models [Bak et al., 1987, 1988; Bak and Chen, 1991; Watkins et al., 2016], which involve state transitions from sub-critial to super-critial toward a fixed point (stable attractor), our SOC model incorporates a dynamic CP actively inducing state changes, allowing adaptive genome regulation in response to stimuli.
7. **A Universality Across Biological Systems**
   This unified genomic mechanism is demonstrated across diverse systems—including HRG- and EGF-stimulated MCF-7 cells [Saeki et al., 2009], atRA- and DMSO-stimulated HL-60 cells [Huang et al., 2005], Th17 cell differentiation [Ciofani et al., 2012], and early embryonic development in mice [Deng et al., 2014] and humans [Yang et al., 2013] - highlighting the robustness and universality of the dynamic criticality model [Tsuchiya et al., 2020, 2022].

Building on these foundational findings, this study aims to clarify the non-equilibrium thermodynamic control of genome expression and differentiate between effective and non-effective dynamics in cell-fate change.

We analyzed temporal gene expression data from MCF-7 cancer cell lines stimulated with Epidermal Growth Factor (EGF), which promotes proliferation without altering cell fate, and Heregulin (HRG), which commits cells after a relatively rapid decay of the gene expression perturbation to differentiate [Zimatore et al., 2021]. By modeling these two processes in terms of open stochastic thermodynamic systems—characterized by exchanges of energy (e.g., heat) and matter (e.g., gases, nutrients, and wastes) with their surroundings and also by inherent randomness—we capture the dynamic and non-deterministic nature of gene regulation influenced by both external and internal factors.

To assess differences in gene expression dynamics, we use Shannon entropy and mutual information as measures of disorder and predictability. Shannon entropy, rooted in information theory, quantifies unpredictability in biological processes and relates to entropy production in nonequilibrium systems, linking informational disorder to energy dissipation. This framework

explains how biological systems maintain order and perform work under stochastic, far-from-equilibrium conditions. Mutual information, on the other hand, captures interdependencies within the gene expression system, revealing regulatory relationships in a quantitative manner. It is essential in stochastic thermodynamics for understanding feedback, control mechanisms, thermodynamic efficiency, and information flow [Shannon, 1948; Adami, 2004; Hübner and Szekely, 2010; Sagawa and Ueda, 2012a, 2012b; Barato and Seifert, 2014].

Maxwell's demon, introduced by physicist James Clerk Maxwell [Maxwell, 1871], is a thought experiment in which a hypothetical "demon" sorts molecules to reduce entropy in a closed system, seemingly violating the second law of thermodynamics. However, extensive studies [Szilárd, 1929; Landauer, 1961; Astumian, 1997; Bennett, 2003; Toyabe et al., 2010; Bérut et al., 2012; Sagawa and Ueda, 2012a, 2012b; Seifert, 2012; Flatt et al., 2023; Annby-Andersson et al., 2024] have demonstrated that Maxwell's demon is not merely a paradox but a key concept for understanding the relationship between information and thermodynamics. These studies show that the demon's ability to measure, store, and process information incurs a thermodynamic cost, thereby preserving the second law. Far from being merely a metaphor, Maxwell's demon embodies a functional principle, validated through experimental systems and biological processes, that underscores the profound connection between information processing and thermodynamic behavior in non-equilibrium systems, including the phenomena of life.

The overview and objectives of our study are as follows:

Understanding complex gene expression networks requires accurate estimation of information-theoretic metrics such as Shannon entropy and mutual information, which measure disorder, predictability, and interdependencies. These metrics are challenging to estimate due to the stochastic nature of gene expression and the complexity of underlying networks.

To address this, we employ Coherent Stochastic Behavior (CSB) through a convergence-based approach [Tsuchiya et al., 2014, 2015]. This enhances the estimation of the CP (Critical Point) location along *nrmsf* (**section 2.1**) and ensures robust identification of CP genes by grouping them on the basis of their expression variability (**section 2.2**). Additionally, this approach improves the robustness of thermodynamic metrics—including entropy and mutual information—which

quantify the dynamics of genomic regulation (**section 2.3**). This methodology enables us to characterize the differences between the genomic mechanisms underlying the action mechanisms of stimuli that are not able to promote cell fate changes (EGF stimulation) and those driving cell-fate changes (HRG stimulation).

Our study focuses on the following objectives:

1. **Open Thermodynamic Modeling and Phase Synchronization** (**section 2.4**): We develop a data-driven approach to model an open stochastic thermodynamic system of MCF-7 cell lines and investigate how order-disorder synchronization between the CP and the Whole Expression System (WES) regulates genome expression under EGF and HRG stimulation.
2. **High-Order Mutual Information** (**section 2.4**): We explore complex interdependencies in synergistic networks within the WES by identifying high-order mutual information.
3. **CP as Maxwell's Demon-Like Rewritable Chromatin Memory** (**sections 2.5 and 2.6**): We examine the CP's role as a Maxwell's demon-like rewritable chromatin memory, clarifying its function in entropy regulation and information flow, thereby deepening our understanding of genomic thermodynamics.

In the Discussion, we explore how these findings pave the way for advancing genome intelligence through autonomous genome computing, offering new strategies for controlling cell fate and developing cancer therapies. The key insights are then summarized in the Conclusion.

2. Results

2.1 A Metric Parameter for Self-Organization of Whole-Genome Expression

To identify the Critical Point (CP) genes, which exhibit critical behavior, we introduce a metric parameter that quantifies the self-organization of time-series whole-genome expression data obtained from both microarray and RNA-Seq datasets (see methodological details in [Tsuchiya et al., 2023b]. This metric parameter is defined by the root mean square fluctuation ($rmsf_i$), representing the standard deviation of a gene's expression levels over time, calculated as follows:

$$rmsf_i = \sqrt{\frac{1}{T}\sum_{j=1}^{T}\left(\varepsilon_i\left(t_j\right) - \langle\varepsilon_i\rangle\right)^2}, \quad (1)$$

where $\varepsilon_i(t_j)$ is the expression level of the ith gene at a specific cell state or experimental time point t_j, $\langle\varepsilon_i\rangle$ is the average expression level of the ith gene over all time points, T is the total number of cell states or experimental time points.

To enable comparisons of gene expression variability across different biological regulations and cell types, we further normalize $rmsf_i$ by the maximum *rmsf* value observed in the entire dataset, resulting in the normalized *rmsf* ($nrmsf_i$). This normalization ensures that $nrmsf_i$ values are comparable across diverse systems [Tsuchiya et al, 2020, 2022].

For each gene expression $\varepsilon_i(t_j)$ across experimental time points, $nrmsf_i$ is first estimated, and then its natural logarithm $ln(\varepsilon_i(t_j))$ is calculated. In this study, "expression" specifically refers to the natural logarithm of the expression value. This transformation reduces fluctuations in expression, thereby facilitating better convergence in the estimation of thermodynamic metrics (see section 2.3).

Note that coherent stochastic behavior (CSB) is key to understanding how self-organized critical (SOC) control of genome expression guides cell fate changes. Applying a logarithmic transformation to gene expression data achieves two goals: 1) capturing scaling response behaviors in SOC control (refer to Fig. 2A in [Tsuchiya et al., 2023b]) and 2) reducing overall noise in higher expression values, though it may amplify small noise near zero. In microarray data—which contain relatively few zero values—this transformation has minimal drawbacks and reliably preserves CSB among gene groups. In contrast, RNA-Seq data, often characterized by numerous zero values, requires an alternative approach: adding small random noise to zero expressions, performing ensemble averaging, and then applying the logarithmic transformation. This ensures that CSB remains invariant (see Note in [Tsuchiya et al., 2023b]).

The biological rationale for selecting *nrmsf* as the ranking parameter is elaborated in [Tsuchiya et al., 2015]. Essentially, gene expression variability serves as a proxy for chromatin flexibility [Zimatore et al., 2021]. Higher variability indicates greater chromatin accessibility and flexibility, which are critical for dynamic gene regulation and responsiveness to cellular signals.

A recent study on MCF-7 cell fate changes, utilizing principal component analysis (PCA) of genome expression profiles [Zimatore et al., 2021], provides further insights into the Self-Organized Criticality (SOC) model of genome expression dynamics. This study revealed that the $nrmsf_i$ value of each gene can be accurately predicted by the principal component scores derived from the temporal correlation matrix of expression profiles. This finding underscores the intrinsic connection between gene expression variability and the underlying regulatory architecture of the genome (see more in section 2.6).

A recent experimental study [Krigerts et al., 2021] has demonstrated that chromatin remodeling plays a pivotal role as the material basis for the SOC control of genome expression. Chromatin remodeling facilitates the dynamic reorganization of chromatin structure, thereby influencing gene accessibility and expression variability. This experimental evidence supports our model, wherein the Critical Point (CP) genes, characterized by high *nrmsf*, act as regulatory hubs orchestrating genome-wide transitions through chromatin flexibility.

2.2 Identifying CP Genes Using the Metric Parameter

The whole-genome mRNA expression dataset is analyzed using the normalized root mean square fluctuation (*nrmsf*; refer to equation (1)) as the metric parameter. Genes are first sorted in descending order of *nrmsf* and then grouped into clusters large enough to capture genome-wide averaging behavior of collective expression dynamics [Tsuchiya et al., 2014, 2015, 2016]. Coherent Stochastic Behavior (CSB) in gene expression emerges when the sample size (n) exceeds 50 [Censi et al., 2011]. As the sample size increases, the group's center of mass (CM) with unit mass converges to a constant value, driven by the law of large numbers. This convergence reflects a nearly balanced inflow and outflow of expression flux within the Whole Expression System (WES) [Tsuchiya et al., 2023b]. To grasp such types of thermodynamic behavior, each group is needed to contain more than 200 genes.

In **Figure 1**, the Critical Point (CP) region is identified through temporal changes in overall expression along the *nrmsf* metric. The CP region demonstrates distinct bimodal behavior, separating high-variance (super-critical) and low-variance (sub-critical) states. **Figure 2** further

illustrates how CSB enables the identification of these distinct response domains, with the CP region acting as a boundary.

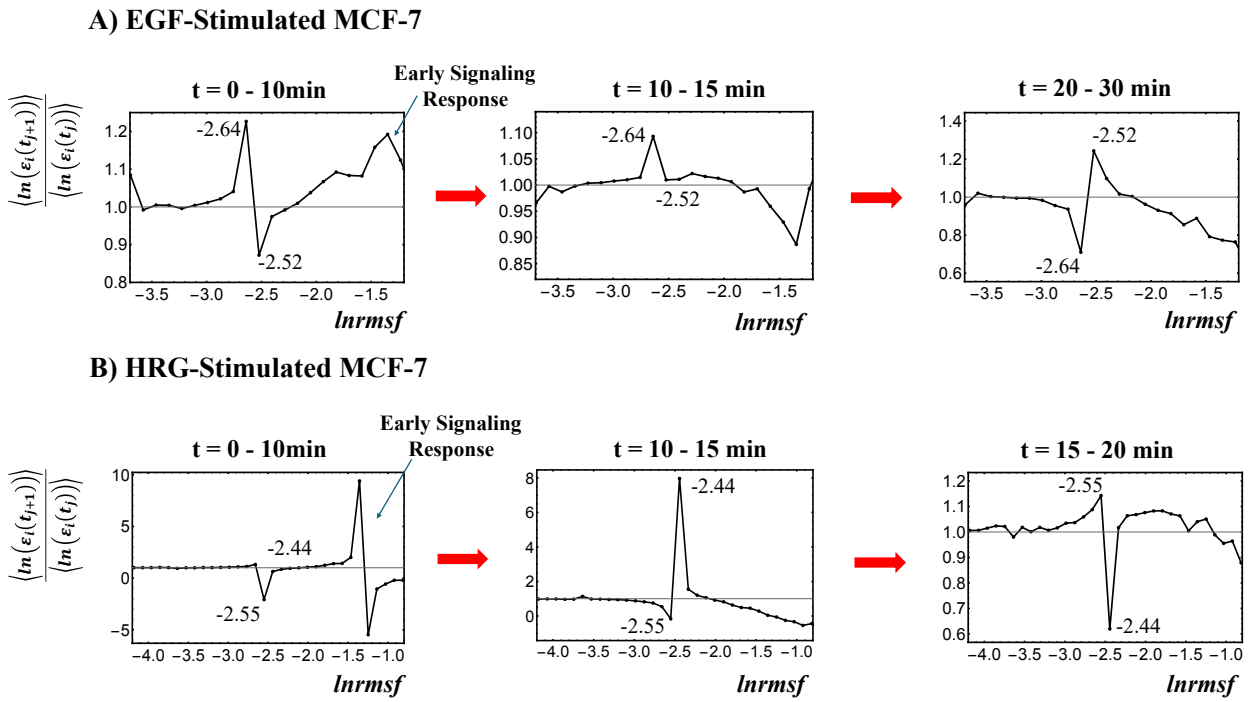

Figure 1: Identification of the Critical Point (CP) Region with Distinct Response Domains. A) EGF-stimulated MCF-7 cells and B) HRG-stimulated MCF-7 cells. According to the *nrmsf* metric parameter, whole expressions are sorted and grouped into 40 equal *nrmsf* ranges, excluding groups with fewer than 200 genes, which typically occur in the highest and lowest regions. The *x*-axis represents the natural logarithm of the average *nrmsf* value, $<nrmsf_i>$ for the ith group, denoted by a black solid dot, while the *y*-axis represents the temporal expression response, calculated as the ratio of the group expression average between consecutive time points, $<ln(\varepsilon_i(t_{j+1}))>/<ln(\varepsilon_i(t_j))>$ (see Note in section 2.1). Under Epidermal Growth Factor (EGF: **A**) stimulation, CP genes exhibit bimodal critical behavior with peaks ranging from -2.64 to -2.52 *ln*(*nrmsf*), while under Heregulin (HRG: **B**) stimulation, the peaks range from -2.55 to -2.44 *ln*(*nrmsf*). The CP region effectively separates high-variance (super-critical: HRG: *ln*(*nrmsf*)> -2.4; EGF: *ln*(*nrmsf*)> -2.5) and low-variance (sub-critical: HRG: *ln*(*nrmsf*)< -2.6; EGF: *ln*(*nrmsf*)< -2.7) responses, highlighting distinct regulatory domains within the genome. The CP region effectively separates high-variance (super-critical) and low-variance (sub-critical) responses, highlighting distinct regulatory domains within the genome. Notably, the CP region includes not only the CP genes themselves but also the surrounding edge genes, further demonstrating its extensive influence.

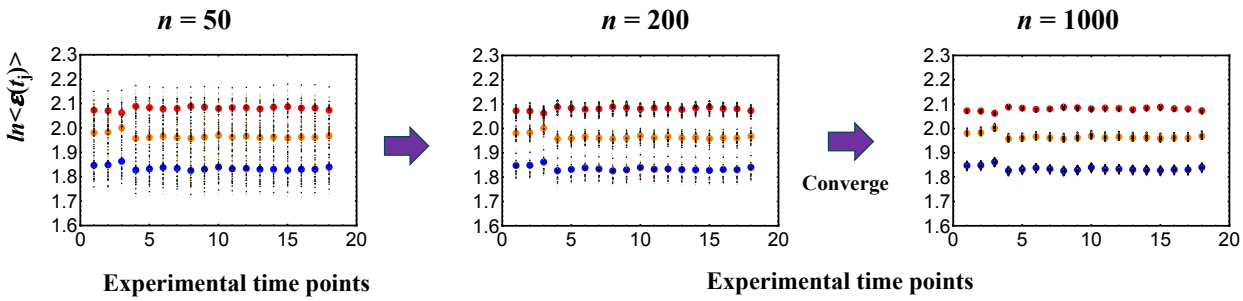

Figure 2: Utilization of Coherent Stochastic Behaviors (CSBs) for Critical-State Attractors. Bootstrapping analysis demonstrates the convergence of the center of mass (CM) of randomly selected gene expressions (sample sizes of n = 50, 200,1000) from critical states. For each random sampling, 40 repetitions are performed across experimental time points, depicted by small dots. This convergence highlights the CM of a critical state acting as an attractor. The large colored dots represent the CM of critical states: red indicates the super-critical state, orange denotes CP-region genes, and blue signifies the sub-critical state. The numbers of gene expressions for the super-critical, sub-critical, and CP-region genes are 10514, 7917, and 3846 (**Figure 1**), respectively. The x-axis corresponds to experimental time points and the y-axis represents the natural logarithm of the average group expression.

2.3 Open Stochastic Thermodynamic Model of MCF-7 Cell Lines

This section presents a stochastic thermodynamic model of MCF-7 breast cancer cell lines, focusing on the interaction between the critical point (CP) gene region and the rest of the whole gene expression system (WES). The remaining genes in WES are collectively referred to as the Peripheral Expression System (PES).

We employ an open thermodynamic model to investigate these interactions, where cells continuously exchange heat and substances such as gases, nutrients, and wastes with their environment. This exchange influences gene expression dynamics. By analyzing entropy variations within the system, we can understand how entropy constrains the organization and stability of gene regulatory networks. This approach reveals the fundamental thermodynamic principles that govern these interactions.

As shown schematically in **Figure 3**, both the CP genes and the PES exchange energy with the external environment (OUT). We analyze an ensemble of the CP genes and the PES within the cancer cell population in terms of entropy and mutual information between the two gene groups, in order to to uncover the thermodynamic properties governing the system.

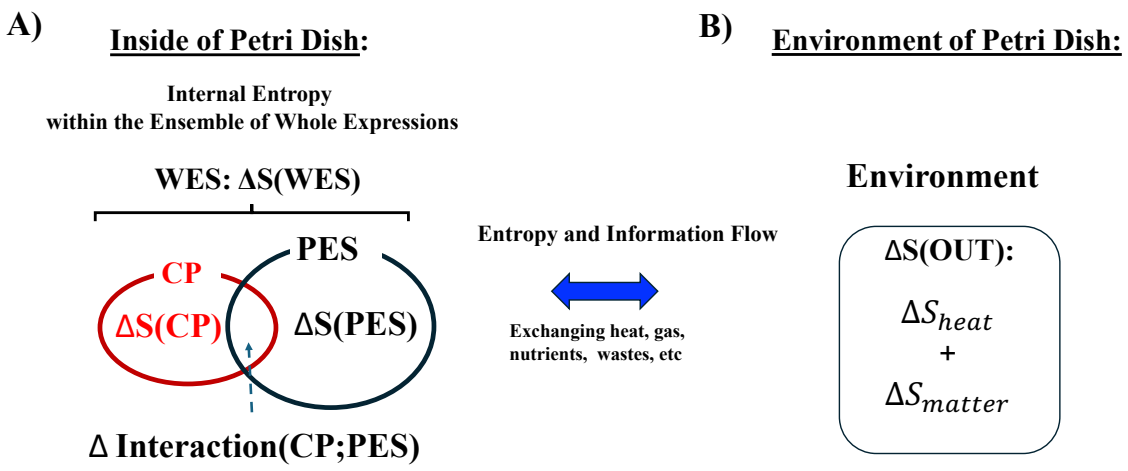

Figure 3: Open Stochastic Thermodynamic Model Setup for MCF-7 Cell Lines.

This schematic depicts an open thermodynamic system for MCF-7 cell lines, where heat, gases, nutrients, and wastes are continuously exchanged with the environment. The system includes the Whole Expression System (WES), which comprises both a set of Critical Point (CP) genes and the remaining genes, referred to as the Peripheral Expression System (PES). Each component has its own entropy: S(WES), S(CP), and S(PES).

A) The total entropy change of WES (ΔS(WES)) is decomposed into changes in CP (ΔS(CP)), PES (ΔS(PES)), and their interaction term (ΔInteraction(CP;PES)). This decomposition enables investigation of how these interaction terms relate to the mutual information ΔI(CP;PES).

B) Entropy exchange with the environment (ΔS(OUT)) is further broken down into contributions from heat (ΔS(heat)) and material exchange (ΔS(matter)).

To estimate entropy and mutual information, the Coherent Stochastic Behavior (CSB) method is applied, revealing coherent gene expression patterns amidst inherent randomness (see **Figure 4**).

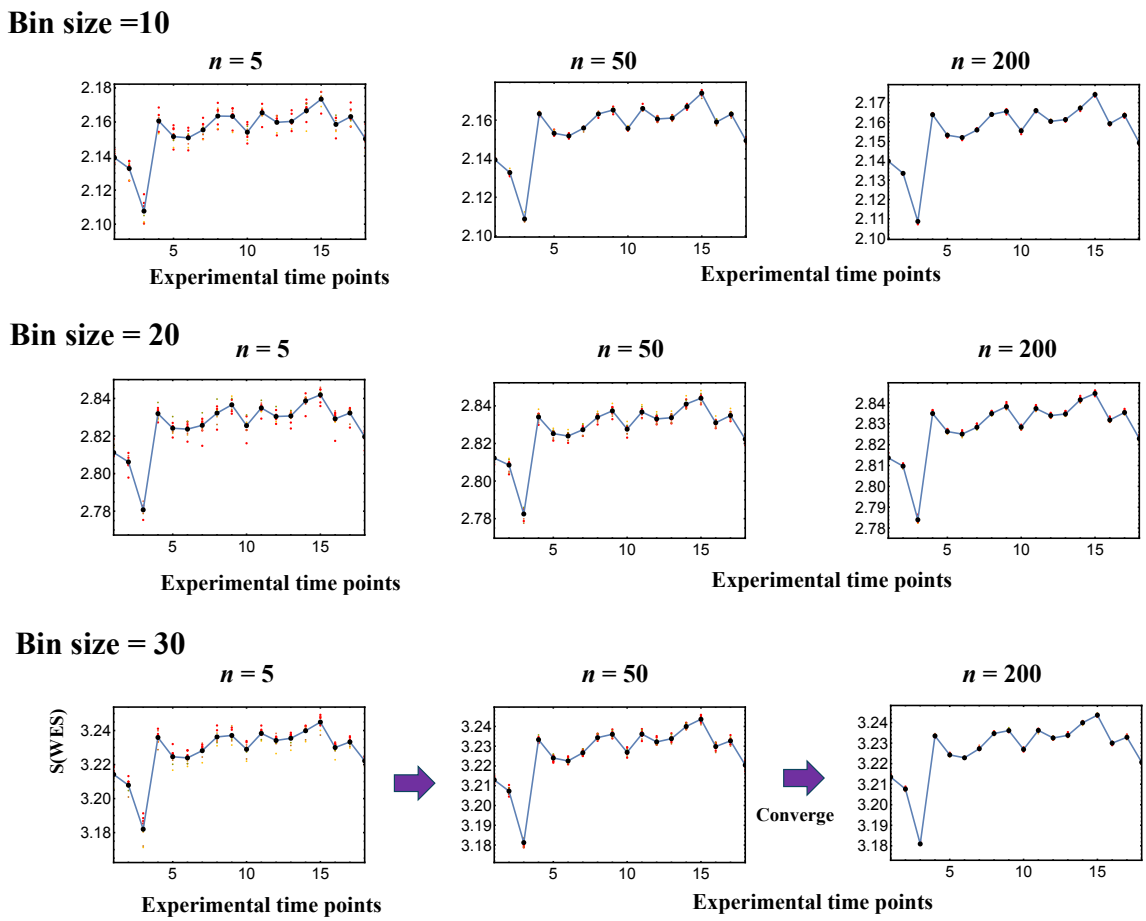

Figure 4: Convergence-based Approach for Robust Estimation of Shannon Entropy. This figure illustrates the convergence of the entropy of the Whole Expression System (*S*(WES)) in HRG-stimulated MCF-7 cancer cells using a bootstrapping analysis. Entropy values are calculated across increasing numbers of repetitions (n = 5, 50, 200) with a fixed sample size of 1000. For each repetition, the probability distribution is estimated using bin sizes of 10, 20, and 30. The bootstrapping process, repeated 10 times, captures fluctuations in average entropy values (small red solid circles), while large black circles represent the average entropy across the 10 repetitions. This analysis highlights two key findings: 1) increasing the number of repetitions improves the robustness of thermodynamic metric estimations (see section 2.3), and 2) different bin sizes introduce a constant offset. This behavior is exactly as expected for entropy as a proper state function: 1) convergence toward the thermodynamic limit and 2) dependence on the chosen sampling resolution. Therefore, we set the bin size to 30 throughout our study (see main text for details). The *x*-axis corresponds to experimental time points, and the *y*-axis represents the value of *S*(WES). The detailed procedure is illustrated in the figure in section 2.6.

In **Figure 2**, increasing the number of genes sampled demonstrates the convergence of the center of mass (CM) of gene expressions, highlighting the attractor behavior of critical states. In contrast, **Figure 4** illustrates that, with a fixed sample size, increasing the number of sampling repetitions through bootstrapping yields a robust estimation of information thermodynamic metrics. This approach leverages CSB to achieve convergence of average values across samplings, thereby stabilizing these estimates. Consequently, it offers a reliable framework for investigating thermodynamic synchronization between CP genes and the Peripheral Expression System (PES), elucidating the thermodynamic principles underlying the genome's dynamic regulatory mechanisms. Additionally, the second thermodynamic condition is considered, accounting for entropy flow between the cell line and its external environment (beyond the confinement of the petri dish), as described below:

1): **Random Sampling**: We repeatedly random sample of genes from the CP, PES and WES datasets, allowing for replacement (bootstrap sampling).

2): **Calculating Entropy**: For each sample, we calculate the Shannon entropy using the following equation:

$$S\left(X(t_j)\right) = -\sum_i P\left(x_i(t_j)\right) ln\left(P\left(x_i(t_j)\right)\right) \quad (2)$$

where $S(\mathrm{X}(t_j))$ is dimensionless; $X(t_j)$ represents $\mathrm{CP}(t_j)$, $\mathrm{PES}(t_j)$ or $\mathrm{WES}(t_j)$ and $P(x_i(t_j))$ is the probability of gene x_i being expressed at t_j.

Note that In **Figure 4**, the probability distributions for gene expression, calculated with different bin sizes, display consistent offsets in the estimation of Shannon entropy dynamics. Similarly, the temporal changes in information thermodynamic metrics reflect constant offsets. These two results point to whole genome expression as an integrated dynamical system. To ensure consistency, we selected a bin size of 30 for the probability distributions, following the Square Root Rule (bin size ~ $\sqrt{n}$ for n: sampling size, refer to [Tsuchiya et al., 2010].

3): **Relating Entropies and High-Order Mutual Information**: We compute the joint entropy $S(\mathrm{CP}, \mathrm{PES})$ at t_j:

$$S\left(CP(t_j), PES(t_j)\right) = -\sum_{x_{i\in CP}, y_j \in PES} P\left(x_i(t_j), y_j(t_j)\right) ln\left(P\left(x_i(t_j), y_j(t_j)\right)\right) \quad (3)$$

where $P(x_i(t_j), y_j(t_j))$ is the joint probability of CP gene x_i and and PES gene y_j being simultaneously expressed at t_j.

The mutual information between CP and PES, I(CP: PES) is given by

$$I\left(CP(t_j); PES(t_j)\right) = S\left(CP(t_j)\right) + S\left(PES(t_j)\right) - S\left(CP(t_j), PES(t_j)\right). \quad (4)$$

The joint entropy S(CP, PES) can also be expressed as internal entropy:

$$S_{internal} = S\left(CP(t_j), PES(t_j)\right) = S\left(CP(t_j)\right) + S\left(PES(t_j)\right) - I\left(CP(t_j); PES(t_j)\right), \quad (5)$$

where the mutual information is subtracted to remove shared information, leaving only the unique and combined uncertainties of the two components. From this point onward, the time t_j will be omitted for simplicity, except when explicitly necessary.

Note that 1) the WES consists of the CP genes and the remaining WES genes (PES), 2) the entropies S(WES), S(CP), and S(PES) are calculated from the full gene set, CP genes, and PES genes, respectively, using the same bootstrap and dimensionless entropy measure, and 3) these entropies implicitly include interactions with the external environment (petri dish; see **Figure 3**).

As shown in **Figure 5**, the difference between S(WES) and S_{internal} (equation (5)) at any experimental time point is not zero, indicating the standard mutual information (referred to as mutual information hereafter) formula (eqaution (4)) do not fully account for all the dependencies in such a complex system like MCF-7 cancer cells:

$$S(WES) \neq S_{internal} = S(CP, PES). \quad (6)$$

This difference arises due to the presence of high-order mutual information [McGill, 1954; Hu, 1962; Rosas et al., 2019] between CP and PES, driven by the complex network of gene interactions,

including cooperative effects, feedback loops, and coordinated regulation across multiple gene networks.

By replacing S(CP,PES) in eqaution (4) with S(WES), the net mutual information including high-order terms, I_{net}(CP; PES) is defined as:

$$I_{net}(CP;PES) = \{S(CP) + S(PES)\} - S(WES). \tag{7}$$

Therefore, from equations (4) and (7), high-order mutual information, I_{high}(CP; PES) can be defined and observed as negative for the entire experimental time:

$$\begin{aligned} I_{high}(CP;PES) &= I_{net}(CP;PES) - I(CP;PES) \\ &= \{S(CP) + S(PES)\} - S(WES) - \{S(CP) + S(PES) - S(CP;PES)\} \\ &= S(CP;PES) - S(WES) < 0 \end{aligned} \tag{8}$$

In **Figure 5**, both EGF and HRG stimulation data reveal that high-order mutual information, I_{high}(CP; PES) < 0 indicates synergistic interactions [Timme et al., 2014]. Here, "synergy" means the combined effect of CP and PES is greater than the sum of their individual effects. Furthermore, in **Figure 6**, it is intriguing that, under both EGF and HRG stimulations, the net mutual information I_{net}(CP; PES) and the higher-order mutual information I_{high}(CP; PES) are nearly equivalent to their corresponding CP entropy S(CP) and joint entropy S(CP,PES), respectively:

$$I_{net}(CP;PES) \sim S(CP) - 0.008 \tag{9}$$

and

$$I_{high}(CP;PES) \sim S(CP,PES) - 3.23 < 0, \tag{10}$$

where biophysical interpretations of these results are described in section 2.4.

4): **Second Law of Thermodynamics:** In our open system—the whole expression system comprising CP genes and PES—the entropy production (σ) quantifies the irreversible processes occurring within the system. Compliance with the second law of thermodynamics mandates that

entropy production must be non-negative ($\sigma \geq 0$), representing the irreversibility inherent in processes like metabolic reactions, molecular interactions, and active transport mechanisms. Dimensionless entropy production (σ) is mathematically defined as the difference between the total change in the WES entropy ($\Delta S(WES)$) and the entropy flow exchanged with the external environment of the petri dish ($\Delta S(OUT)$):

$$\sigma = \Delta S(WES) - \Delta S(OUT) \geq 0 \,. \tag{11}$$

The change in entropy of the outside environment, $\Delta S(\mathrm{OUT})$ is given by

$$\Delta S(OUT) = \Delta S_{heat} + \Delta S_{matter}, \tag{12}$$

where

$$\Delta S_{heat} = \frac{Q}{T} \tag{13}$$

represents the entropy change due to heat (Q) exchange at a temparature (T = 37 °C), and $\Delta S_{\mathrm{matter}}$ is the net entropy exchange associated with the inflow and outflow of substances:

$$\Delta S_{matter} = \sum_{out} n_{out} \cdot s_{out} - \sum_{in} n_{in} \cdot s_{in}, \tag{14}$$

where n_{in} and s_{in} represent the molar quantity and molar entropy of inflowing substances, and n_{out} and s_{out} for outflows.

Cells generate heat through metabolic activities (e.g., ATP synthesis, substrate oxidation), exchange nutrients (e.g., glucose, amino acids) and waste products (e.g., CO_2, lactate) with the environment.

Therefore, we obtain the second law condition for the system:

$$\sigma = \Delta S(WES) - \left(\frac{Q}{T} + \Delta S_{matter}\right) \geq 0. \tag{15}$$

Internal entropy production σ must be non-negative ($\sigma \geq 0$) to satisfy the second law of thermodynamics. This ensures that all irreversible processes within the cell culture contribute to an overall increase in entropy.

2.4 Genomic-Thermodynamic Phase Synchronization Between CP Genes and the Whole Expression System

Based on the stochastic thermodynamic model, our results show in EGF-stimulated and HRG-stimulated MCF-7 cells as below:

In EGF-stimulated MCF-7 cells:

A) Dissipative Thermodynamic Synchronization of Order-Disorder Phases

EGF stimulation activates EGFR in MCF-7 cells, triggering the MAPK/ERK pathway for gene regulation and the PI3K/AKT pathway for survival, driving proliferation within the first 10 minutes [Saeki et al., 2009]. This signaling is associated with the largest changes in the entropy of the Critical Point (CP) region genes, S(CP), and the Peripheral Expression System, S(PES), as evident in the first two time points (0–10 min) in **Figure 5A**. The temporal profiles of S(CP) and S(PES) reveal phase synchronization between CP and PES, characterized by coordinated shifts between ordered and disordered phases (**Figure 6A**). This synchronization is fundamentally driven by their net mutual information I_{net}(CP;PES), which combines mutual information and higher-order interactions.

As an open system, the increases in entropy within CP and PES adhere to thermodynamic principles, reflecting exchanges of heat and matter with the environment (see section 2.3). The rising net mutual information I_{net}(CP;PES), scaling with CP entropy S(CP), indicates that as CP's complexity increases, its influence on PES strengthens, promoting greater integration between the two subsystems.

Meanwhile, the negative higher-order mutual information, I_{high}(CP;PES)< 0, scaling with the joint entropy, S(CP,PES) highlights synergistic interactions between CP and PES. This synergy fosters emergent properties and coordinated behavior, demonstrating that open

systems can achieve local ordering and integration through environmental exchanges: a hallmark of dissipative, nonequilibrium thermodynamics.

B) **Dynamic Equilibrium Underpinning Coherent Stochastic Behavior (CSB)**

In **Figure 5A**, the entropy of the whole expression system S(WES) exhibits small fluctuations around an average value of 3.23, with variations within the range of 2.26×10^{-2}. These fluctuations are an order of magnitude smaller than those observed for S(CP,PES) and I_{net}(CP;PES). This suggests that, although significant exchanges occur between WES and the external environment (outside the petri dish), the entropy within WES remains relatively stable. Such stability suggests an effective thermodynamic and informational balance between WES and its environment, preserving dynamic equilibrium during EGF stimulation. This observation aligns with previous findings from expression flux analysis [Tsuchiya et al., 2020, 2022], indicating a biophysical basis that upholds the law of large numbers. This balance ensures Coherent Stochastic Behavior (CSB), where the collective behavior of the system remains consistent despite the stochastic nature of individual molecular interactions.

In HRG-stimulated MCF-7 cells:

A) i) Dissipative Thermodynamic Synchronization of Order-Disorder Phases

Figure 5B shows that in HRG-stimulated MCF-7 cells, S(PES) has higher temporl Peason correlation with S(CP) indicating stronger phase synchronization between the CP and PES compared to EGF-stimulated cells (**Figure 5A**). This enhanced synchronization suggests a more coordinated interaction between CP and PES under HRG stimulation, indicating robust thermodynamic coupling within the system.

ii) Activation of the CP as a Maxwell Demon: Distinguishing Cell-Fate from Non-Cell-Fate Processes

Unlike EGF stimulation, which induces a large initial disorder change within the first 0–10 minutes, HRG stimulation triggers distinct order-disorder transitions in the entropy of both S(CP) and S(PES) during the 10–20 minute period (**Figure 5B**). This marks a critical transition aligning with findings from PCA analysis [Zimatore et al., 2021] and expression flux analysis [Tsuchiya et al., 2020, 2022].

Thermodynamically, this transition involves the CP acting analogously to a Maxwell demon (see detailed analysis in sections 2.5 and 2.6), where it induces feedback to the PES and orchestrates a genomic avalanche that drives cell-fate change.

From a biological standpoint, compared to EGF stimulation, HRG stimulation activates the ERK/Akt pathway within 5 to 10 minutes, leading to a ligand-specific biphasic induction of AP-1 complex components - including c-FOS, c-JUN, and FRA-1 - as well as the induction of the key transcription factor c-MYC [Nagashima et al. 2007; Saeki et al., 2009]. This cascade produces a pulse-like genome-wide perturbation at 15–20 minutes, marked by the activation of oscillating-mode genes (OMG) - genes with high scores on the second principal component. These genes emit large expression fluxes to both the CP and the genome attractor (GA), facilitating their synchronization within the OMG–CP–GA network [Tsuchiya et al., 2023a].

At 15–20 minutes, this critical transition is followed by a peak in c-MYC expression at 60 minutes [Krigerts, et al., 2021], resulting in extensive gene amplification. Beyond this point, entropy changes exhibit steady fluctuations with damping behavior, as also observed in both PCA and expression flux analyses. This behavior indicates balanced large-scale energy flows that sustain cellular homeostasis.

The critical distinction between HRG and EGF stimulation lies in the activation of the CP as a Maxwell demon under HRG. This unique activation drives the critical transition and ensures the precise coordination necessary for cell-fate determination.

In summary, as shown in **Figure 6**, phase synchronization ensures that when S(CP) increases, the net mutual information also rises, highlighting the growing influence of CP on PES. The system operates through a dual mechanism: the CP-PES synchronization serves as the primary mode of interaction, while higher-order synergy introduces additional complexity and robustness. This coupling allows CP to efficiently regulate PES dynamics, particularly during critical transitions in HRG-stimulated MCF-7 cells, driving shifts to a new genomic state.

In contrast, the higher-order component, $I_{\mathrm{high}}(\mathrm{CP;PES}) < 0$, which scales with the joint entropy $S(\mathrm{CP,PES})$ as $I_{\mathrm{high}}(\mathrm{CP;PES}) \sim S(\mathrm{CP,PES})$ -3.23, represents the synergistic gain from higher-order interaction. This interaction plays a pivotal role in reducing the overall entropy of the CP-PES system. Both EGF and HRG stimulations show the same constant shifts of -3.23 in $S(\mathrm{CP,PES})$ and

- 0.008 in S(CP), indicating these as defining features of MCF-7 cancer cells. This balance between pairwise synchronization and higher-order synergy supports efficient and robust regulation of gene expression during dynamic cellular processes.

These findings on EGF- and HRG-stimulations demonstrate that changes in entropy and net mutual information effectively serve as indicators of fundamental cellular processes, including the activation of signaling pathways, occurrence of critical transitions, and synchronization of genome expression. Adopting this thermodynamic perspective enriches our understanding of how different stimuli orchestrate complex regulatory networks within cells.

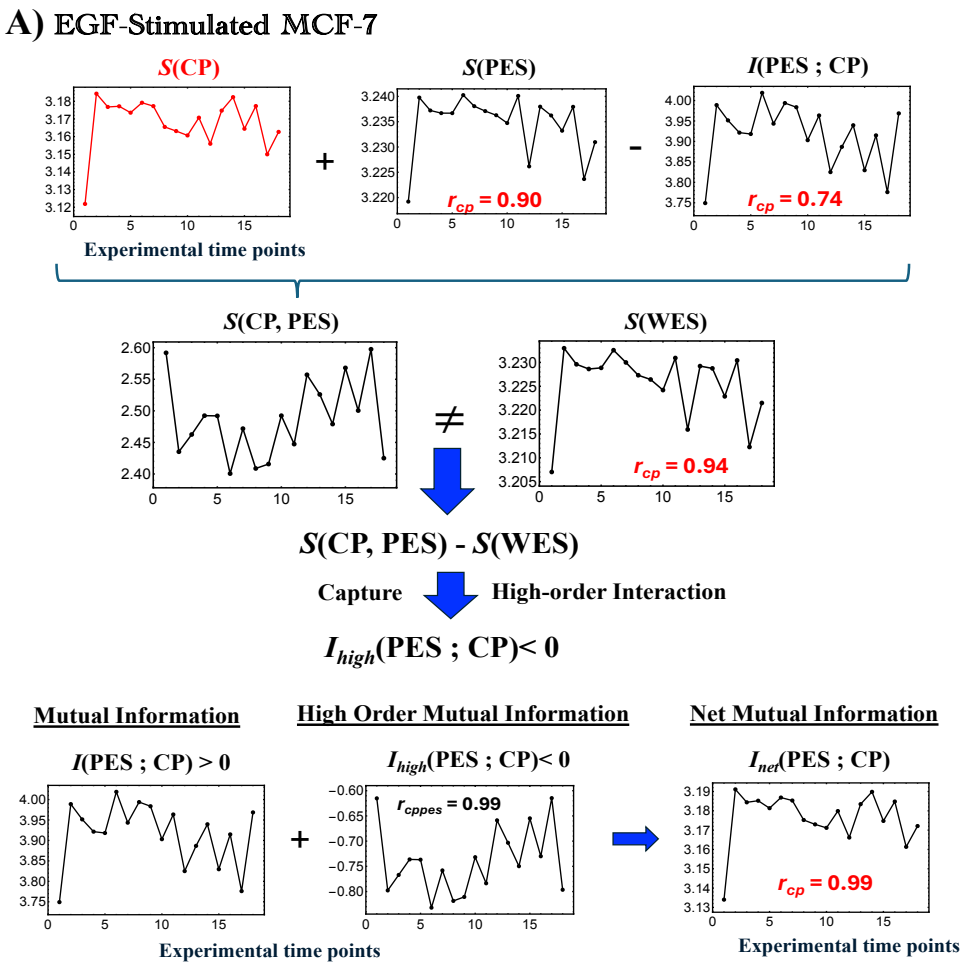

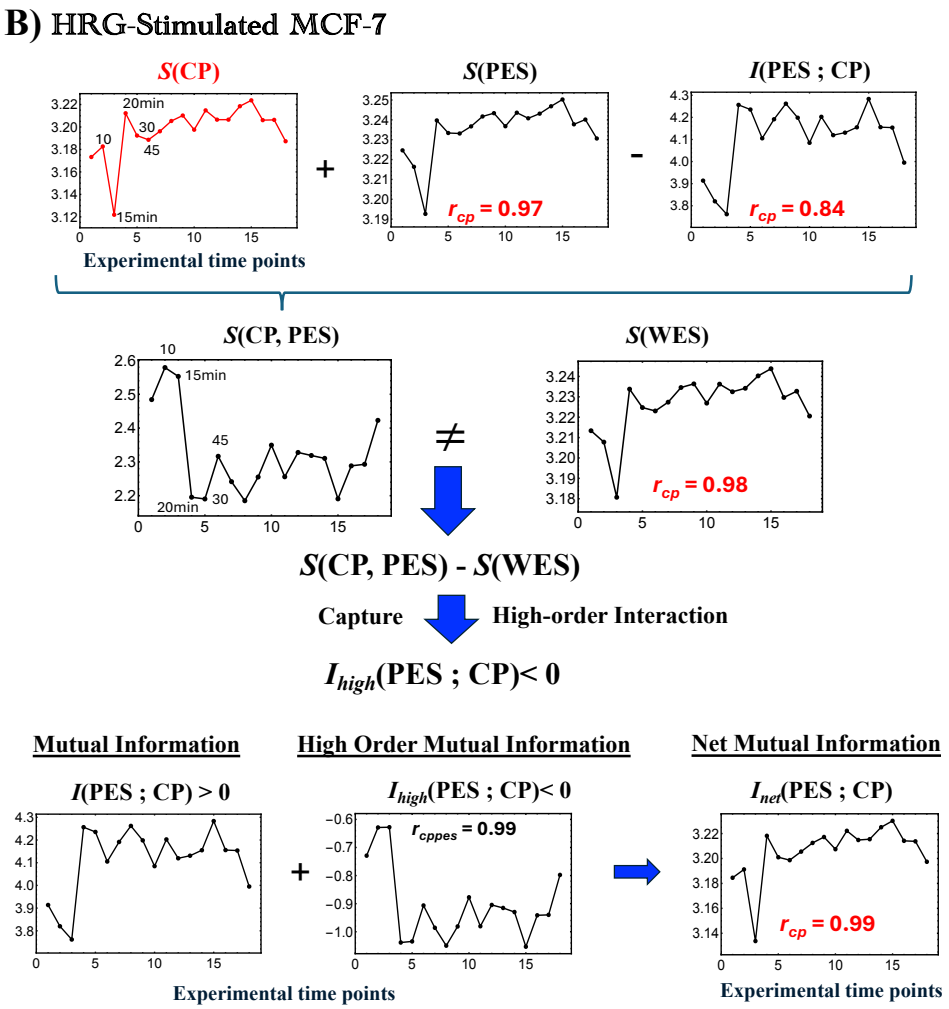

Figure 5. Thermodynamic Phase Synchronization and Higher-Order Mutual Information in MCF-7 Cells. A) EGF-stimulation and **B)** HRG-stimulation. Using a bootstrapping approach with 500 repetitions and a sample size of 1,000, we confirmed that Coherent Stochastic Behavior (CSB) robustly applies to several key entropy measures. These include the entropy of the entire genes, WES (S(WES)), the entropy of CP genes (S(CP)), the entropy of PES genes (S(PES)), the joint entropy of CP and PES genes (S(CP, PES)), and the mutual information between CP and PES genes (I(CP; PES)). For both EGF and HRG stimulations, the difference between S(WES) and S(CP, PES) reveals negative higher-order mutual information, denoted as I_{high}(CP; PES) (see equation (8)), showing an almost perfect temporal Pearson correlation with S(CP,PES) (r_{cppes}). The net mutual information, I_{net}(CP; PES) (see equation (7)), exhibits a near-perfect temporal correlation with the dynamics of S(CP) (r_{cp}). This negative higher-order mutual information captures synergetic interactions within the WES. These findings demonstrate PES and WES exhibit strong synchronization of order-disorder phases with CP ($r_{\text{cp}} > 0.9$), reflected in the behavior of I_{net}(CP; PES) in MCF-7 cells. The y-axis represents the measured values, while the x-axis shows time points

at 0, 10, 15, 20, 30, 45, 60, 90, 120, 180, 240, 360, 480, 720, 1,440, 2,160, 2,880, and 4,320 minutes. For further details, refer to the main text.

A) **Phase synchronization:** EGF-stimulation

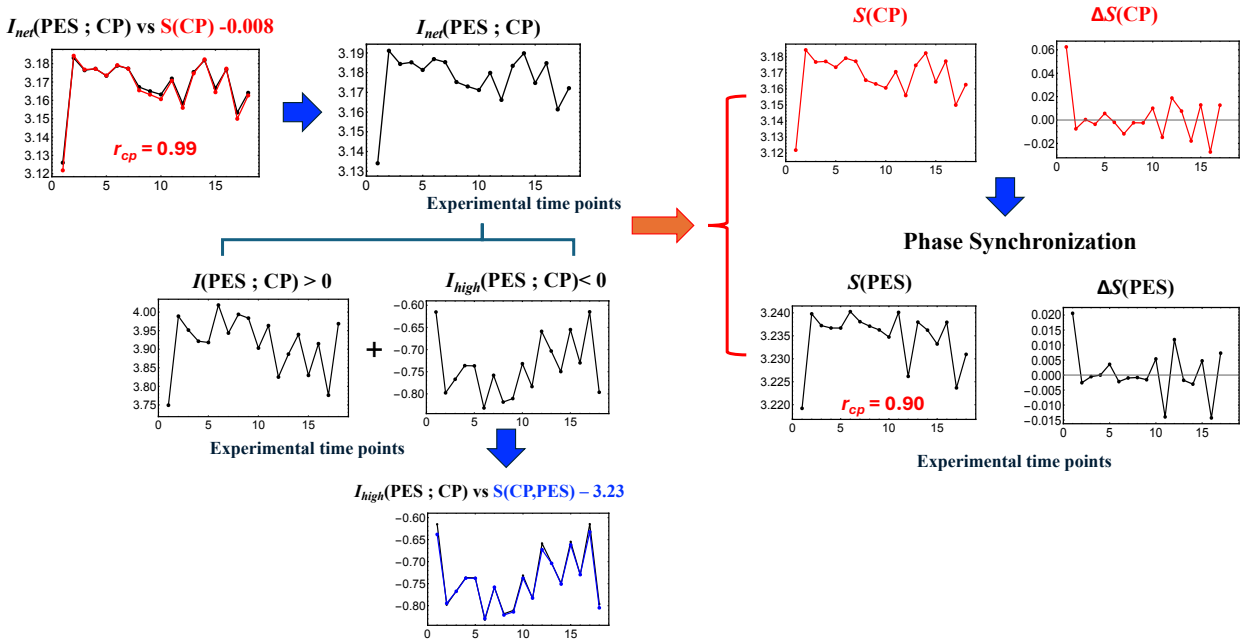

B) **Phase synchronization:** HRG-stimulation

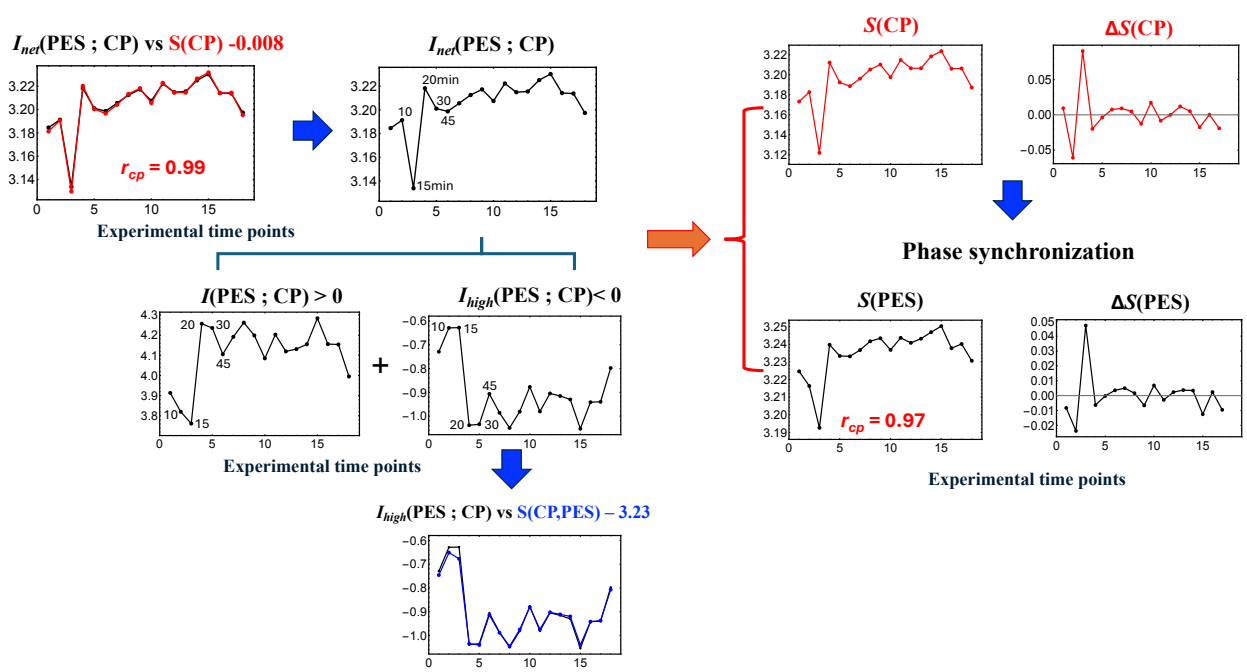

Figure 6: Thermodynamic Phase Synchronization of CP with the Rest of WES (PES). A) EGF stimulation. B) HRG stimulation. The net mutual information, comprising mutual information and higher-order information, scales with the CP entropy dynamics (see equation (9)), supporting fundamental phase synchronization between CP and PES. The higher-order information aligns with the joint entropy S(CP,PES) (equation (10)) and becomes negative, indicating synergistic interactions within the WES (see main text for details).

2.5 CP Acts as Maxwell's Demon in Early HRG-Signaling Response

In the previous section, we demonstrated that MCF-7 cell population exhibits thermodynamic phase synchronization between the Critical Point (CP) and the rest of the WES (Peripheral Expression System, PES), along with their net mutual information. HRG stimulation induces a distinct critical transition between ordered and disordered phases from 10 to 20 minutes, in contrast to the early disordered response observed with EGF during the 0–10 minute timeframe. As shown in **Figures 5B** and **6B**, the CP functions similarly to Maxwell's demon [Parrondo et al., 2015], controlling information flow and maintaining adaptable chromatin states (see section 2.7 for more details).

The CP, functioning as a Maxwell's demon, orchestrates gene expression and cell fate through three distinct phases:

1. **Phase 1: Preparation (10–15 minutes)** - In this phase, the CP, acting as Maxwell's demon, synchronizes with the PES to minimize the entropies of both CP and PES genes, establishing their initial states.
2. **Phase 2: Measurement (15–20 minutes)** - In this phase, synchronization between the CP and PES initiates the measurement process, leading to the highest increases in entropy for both the CP and PES and the largest decrease in higher-order mutual information. The enhanced synergy between the CP and PES reduces redundancy, ensuring an efficient measurement process.
3. **Phase 3: Feedback and Critical Transition (20–30 minutes)** - Utilizing the net information obtained from Phase 2, the CP reorganizes and provides feedback to the PES,

triggering a critical transition in the gene expression system. This feedback-driven reorganization reduces system entropy, driving the system into a new ordered state.

Further details are provided below:

Phase 1: Preparation (10–15 minutes)

Minima of Entropies and Maximum of Higher-Order Mutual Information at 15 Minutes
Between 10 and 15 minutes post-HRG stimulation, the preparation of the CP, functioning analogously to Maxwell's demon, occurs through the minimization of three key metrics: the entropies S(CP), S(PES), and the net mutual information I_{net}(CP;PES). At 15 minutes, these minima are achieved through phase synchronization between the CP and PES, driven by I_{net}(CP;PES). While I_{net}(CP;PES) reaches its minimum due to a decrease in mutual information I(CP;PES), the higher-order mutual information I_{high}(CP;PES) remains at its maximum, indicating stable complex interactions.

Biologically, this synchronization results in the sustained up-regulation of AP-1 complex genes and the coordinated activation of their downstream targets, ensuring proper assembly and functionality of the AP-1 complex components (see section 2.4).

Phase 2: Measurement Phase (15–20 Minutes)

1. Highest Increases in CP Entropy, PES Entropy, and Net Mutual Information

As shown by the data points at 15 and 20 minutes (second and third points) in **Figure 5B** (or **Figure 6B**), during the Measurement Phase, CP genes acquire the highest amount of information about the PES. To process and store this information, the entropy of the CP, S(CP), increases due to the thermodynamic costs associated with information processing.

During this phase, both the net mutual information I_{net}(CP;PES) > 0 and the mutual information I(CP;PES) > 0 exhibit their largest increases from the minima at 15 minutes. In contrast, the higher-order mutual information I_{high}(CP;PES) < 0 shows its largest decrease from the previous maximum, suggesting reduced redundancy and enhanced synergy between CP and PES.

Furthermore, the higher-order mutual information I_{high}(CP;PES) < 0 scales with the joint entropy S(CP,PES). This relationship suggests that as the total uncertainty or disorder of the combined system increases, reflected by the joint entropy, the higher-order interaction between CP and PES becomes more synergistic, as indicated by a more negative I_{high}(CP;PES). Despite the rise in overall uncertainty, this enhanced synergy between CP and PES reduces redundancy and focuses on essential interactions, enabling an efficient measurement process.

The synchronized metrics in Phase 2 lay the foundation for the feedback process in Phase 3, driving the system's critical transition to a new cell state.

Note: Typically, in measurement scenarios [Parrondo et al., 2015], the entropy of the measured system, S(PES), decreases as it loses information to the CP, increasing internal order. However, during this phase, S(PES) instead increases. This rise is due to phase synchronization between the CP and PES, during which the PES absorbs energy from the environment. This energy, which includes heat, free energy, or chemical energy such as from nutrients or reactants, offsets the entropy reduction caused by information loss to the CP. This process demonstrates that phase synchronization occurs through exchanges with the external environment of the petri cell (see section 2.4).

Phase 3: Feedback and critical transition

1. Initiation of Critical Transition (20–30 Minutes):

Between 20 and 30 minutes, the decrease in CP entropy induces a corresponding reduction in PES entropy through phase synchronization between the CP and PES, mediated by exchange entropy and information flow with the environment. During this time, the net mutual information I_{net}(CP;PES) > 0 also decreases, while the higher-order mutual information I_{high}(CP;PES) < 0 remains unchanged. This suggests that the CP is effectively using the information obtained in Phase 2 to guide the PES through a critical transition. Notably, the timing of feedback by the CP at 20 minutes coincides with the onset of a genome-wide transition, as demonstrated by expression flux analysis [Tsuchiya et al., 2020, 2022] and PCA analysis [Zimatore et al., 2021].

2. Stabilization into New States After 30 minutes:

After 30 minutes, temporal changes in *S*(CP) and *S*(PES), along with dynamics of the net mutual information, fluctuate, suggesting that both CP and PES are settling into stable, reorganized states. Note that during this period, the bimodal CP dissipates between 30 and 45 minutes (see section 2.6). This stabilization marks a coordinated gene expression system following the critical transition.

Throughout Phases 1 to 3, the CP functions analogously to Maxwell's demon, selectively regulating gene expression associated with chromatin states. This intricate process underscores the balance between information processing and entropy control within the HRG-stimulated MCF-7 cancer genome. By managing entropy and leveraging high-order mutual information, the CP orchestrates gene regulation, facilitates cellular transitions, and maintains epigenetic memory, providing valuable insights into the mechanisms of gene regulation and cellular behavior in cancer.

2.6 Maxwell's Demon Functioning as Rewritable Chromatin Memory

J. Krigerts et al. [Krigerts et al., 2021] recently investigated experimentally critical transitions in chromatin dynamics during early differentiation in HRG-stimulated MCF-7 breast cancer cells, focusing on pericentromere-associated domains (PADs). They identified two key critical transitions:

1. **First Critical Transition (15-20 Minutes)**: Following HRG treatment, PADs undergo a "burst," dispersing from their clustered state near the nucleolus. This dispersal coincides with the activation of early response genes, such as *c-fos*, *fosL1*, and *c-myc*, which initiate the differentiation process. During this phase, repressive chromatin structures unravel, and active chromatin regions become more accessible, marking a significant step in genome reorganization. The timing of the critical transition coincides with our expression flux analysis [Tsuchiya et al., 2020, 2022] and PCA [Zimatore et al., 2021] aligns with the findings of our current study.
2. **Second Critical Transition (Around 60 Minutes):** The second transition involves further chromatin alterations, including increased transcription of long non-coding RNAs

(lncRNAs) from PADs. This supports additional chromatin unfolding and genome rewiring, which are essential for establishing and maintaining differentiation, ultimately determining a stable and functional cell fate.

In this section, we explore the thermodynamic mechanisms underlying these two critical transitions in chromatin dynamics. To achieve this, we analyze the metric parameter *nrmsf* (equation (1)), which indicates the self-organization of the whole expression system (WES) into distinct response domains (critical states) separated by a critical point (CP) (**Figure 1**). This parameter quantifies the temporal variability of gene expression as a time-independent measure.

Zimatore et al. [Zimatore et al., 2021] demonstrated that *nrmsf* effectively captures the variability in gene expression over time. They further showed that principal component (PC) scores derived from temporal whole expression data accurately predict each gene's *nrmsf* value. The fluctuation modes PC2 and PC3 correlate with chromatin's structural flexibility, which are strongly associated with chromatin folding and unfolding during the cell-fate-guiding critical transition in HRG-stimulated MCF-7 cells. Notably, the substantial (one-order-of-magnitude) increase in the proportion of variance explained by PC2—the primary direction of displacement from the genome attractor (GA)—coincides with the splitting of peri-centromeric bodies and subsequent chromatin unfolding, making new genomic regions accessible to polymerases [Krigerts et al., 2021]. Given that PC2 closely mirrors changes in *nrmsf* for oscillating mode genes (OMGs) [Tsuchiya et al., 2023a], these findings allow us to connect chromatin dynamics with thermodynamic properties such as Shannon entropy.

To formulate the Shannon entropy associated with chromatin dynamics, we transform the original gene expression probability distribution into an *nrmsf* probability distribution (see Appendix for mathematical description). **Figure 7** illustrates this workflow: starting with the raw expression data, we systematically bin gene expression values into m discrete *nrmsf* categories. These categories serve as 'logical states,' while the actual gene expression values populating each bin represent the 'physical states' embedded within those logical categories.

This approach aligns with the concept of entropy decomposition into logical and physical states, as discussed by Maroney [Maroney, 2009] in the context of generalizing Landauer's principle. By

establishing *nrmsf* bins as logical states, we create a structured, higher-level framework that organizes the more granular expression levels (physical states). In other words, the logical states (i.e., *nrms*f bins) capture the distribution of uncertainty at a coarser scale, while the physical states (the actual gene expression values within each bin) account for the residual uncertainty at finer resolution.

To ensure the robustness of our entropy estimates, we employ a convergence-based approach described in **Figure 4**. This method stabilizes the assessment of uncertainty by redistributing the fundamental entropy element, $-p(x_i(t_j))ln(p(x_i(t_j)))$, across the *nrmsf* bins. Each individual expression value ($x_i(t_j)$) contributes to the entropy at the logical (bin) level, allowing us to map local gene expression dynamics onto the *nrmsf* probability distribution.

Through this transformation, we gain insights into how chromatin state changes influence the distribution of gene expression. By viewing entropy both at the logical (*nrmsf* bin) and physical (individual expression values) scales, we move beyond raw probability distributions to an information-theoretic description that captures dynamic variability and regulatory mechanisms at play in chromatin dynamics.

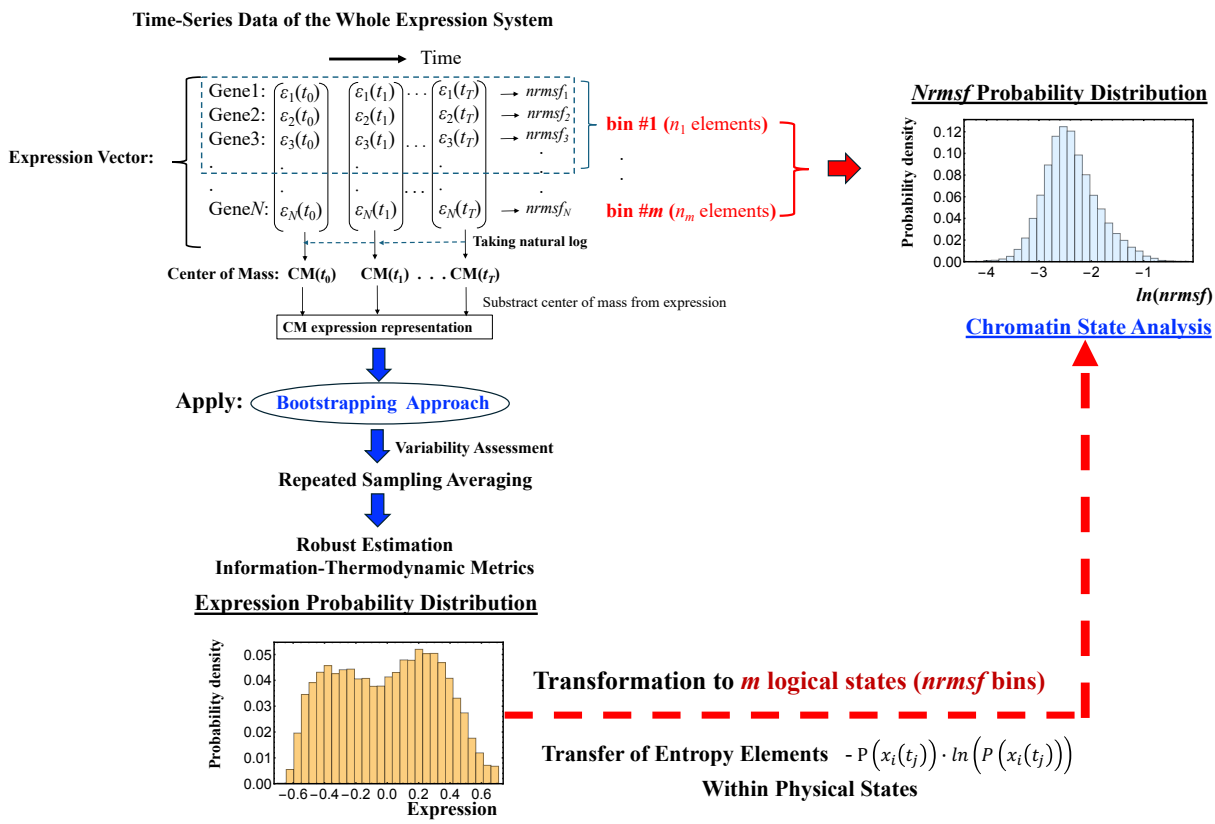

Figure 7: Transforming Gene Expression Distributions into *nrmsf* Probability Distributions: An Information-Theoretic Approach. This figure illustrates the workflow for transforming gene expression probability distributions into *nrmsf* probability distributions, reflecting entropy changes associated with chromatin states. The process begins with temporal gene expression data of the whole expression system (WES), which includes the CP as the regulatory hub and the peripheral expression system (PES) (refer to **Figure 1**). Mutual information metrics, $I_{\text{net}}(\text{CP;PES}) = I(\text{CP;PES}) + I_{high}(\text{CP;PES})$, are calculated to quantify the interaction and coherence between these subsystems, providing an information-theoretic perspective on gene regulation (see **section 2.3**). A bootstrapping approach (**Figure 4**) is applied to assess the variability and uncertainty of these metrics, ensuring robustness in the analysis. Finally, entropy elements, represented as $-p(x_i(t_j))ln(p(x_i(t_j)))$, are transformed into an *nrmsf*-based probability distribution. The *nrmsf* bins represent logical states, while the original gene expression values within each bin correspond to the underlying physical states. By incorporating this logical/physical state perspective, the transformation reveals dynamic variability and chromatin state changes. For additional details, refer to **Figure 8**.

Figure 8 depicts the temporal variations in Shannon entropy linked to chromatin dynamics across the WES for EGF- and HRG-stimulated MCF-7 cells:

1. **EGF-stimulated MCF-7 cells: Figure 8A** illustrates the temporal changes in Shannon entropy associated with chromatin dynamics in EGF-stimulated MCF-7 cells. Within the specified range ($-2.64 < ln(nrmsf) < -2.52$; **Fugure 1**), a bimodal coherent pattern regarding entropy changes occasionally appears, suggesting CP-like (critical point-like) behavior in chromatin organization. In these instances, positive entropy changes ($\Delta S > 0$) are associated with chromatin unfolding, while negative entropy changes ($\Delta S < 0$) are associated with chromatin folding.

   Although these CP-like bimodal patterns emerge at certain intervals—such as during the 0–10 and 20–30 minute time frames—they dissolve and reappear without resulting in a sustained critical transition or a change in cell fate. This indicates that the necessary conditions for activating a Maxwell's demon-like mechanism to drive such transitions are not fully met. Notably, these fluctuations in chromatin dynamics is driven by CP-PES phase synchronization (section 2.4), emphasizing the role of thermodynamic interactions in maintaining dynamic chromatin states despite the absence of a critical transition.
2. **HRG-stimulated MCF-7 cells: Figure 8B** shows that, in HRG-stimulated MCF-7 cells, a CP-like bimodal pattern of ($-2.55 < ln(nrmsf) < -2.44$; **Figure 1**) forms during the initial 0–10 minutes of HRG signaling. Between 10–30 minutes, a global coherent fold-unfold transition occurs centered around $ln(nrmsf) = -3.11$ to -3.04. This phase corresponds to the activity of Maxwell's demon-like behavior (see section 2.5), acting as a rewritable chromatin memory and reflecting changes in double-well potential profiles (refer to **Figure 9**). Subsequently, between 30–45 minutes, the CP pattern dissolves, likely preparing the system for a new stable genomic state of the WES. At 60–90 minutes, CP formation is observed again, suggesting that a cell fate change occur as the second transition described by Krigerts et al. [Krigerts et al., 2021]. After 90 minutes, the formation and dissolution of CP bimodal patterns continue at certain intervals, resembling the pattern seen in EGF-stimulated MCF-7 cells.

Using the *nrmsf* metric, Shannon entropy reveals chromatin folding and unfolding dynamics. EGF stimulation repeatedly dissolves and reinitiates reversed CP bimodal pattern formations without inducing cell fate changes, while HRG stimulation facilitates stable CP formation and cell fate transitions driven by Maxwell's demon-like chromatin memory at 10-30 min. The CP's role—measuring genomic states, orchestrating entropic and informational dynamics, and reorganizing chromatin—demonstrates its active function in encoding, decoding, and re-encoding chromatin configurations. This process aligns with the concept of memory storage and rewriting within a dynamically regulated, thermodynamically controlled genomic landscape (**Figure 9**).

A) EGF-Stimulation

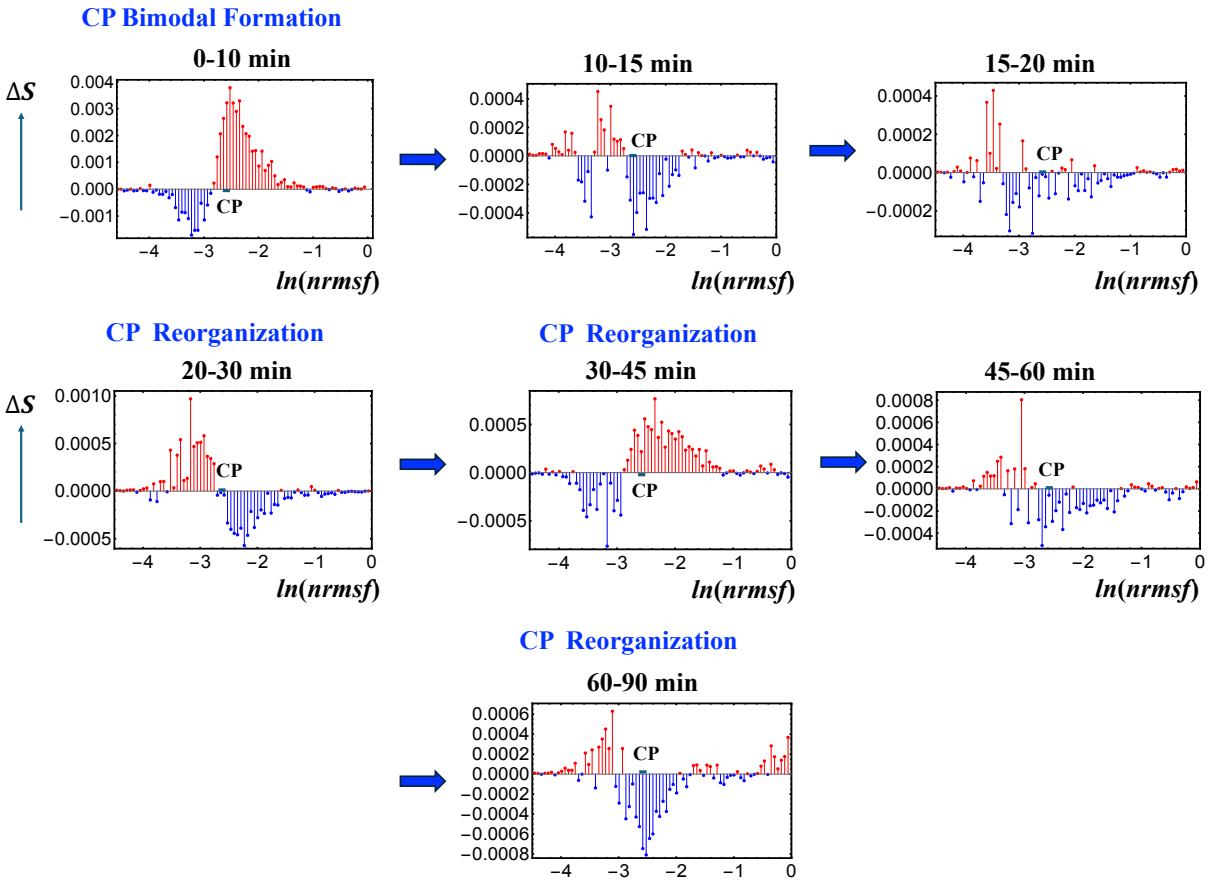

B) HRG-Stimulation

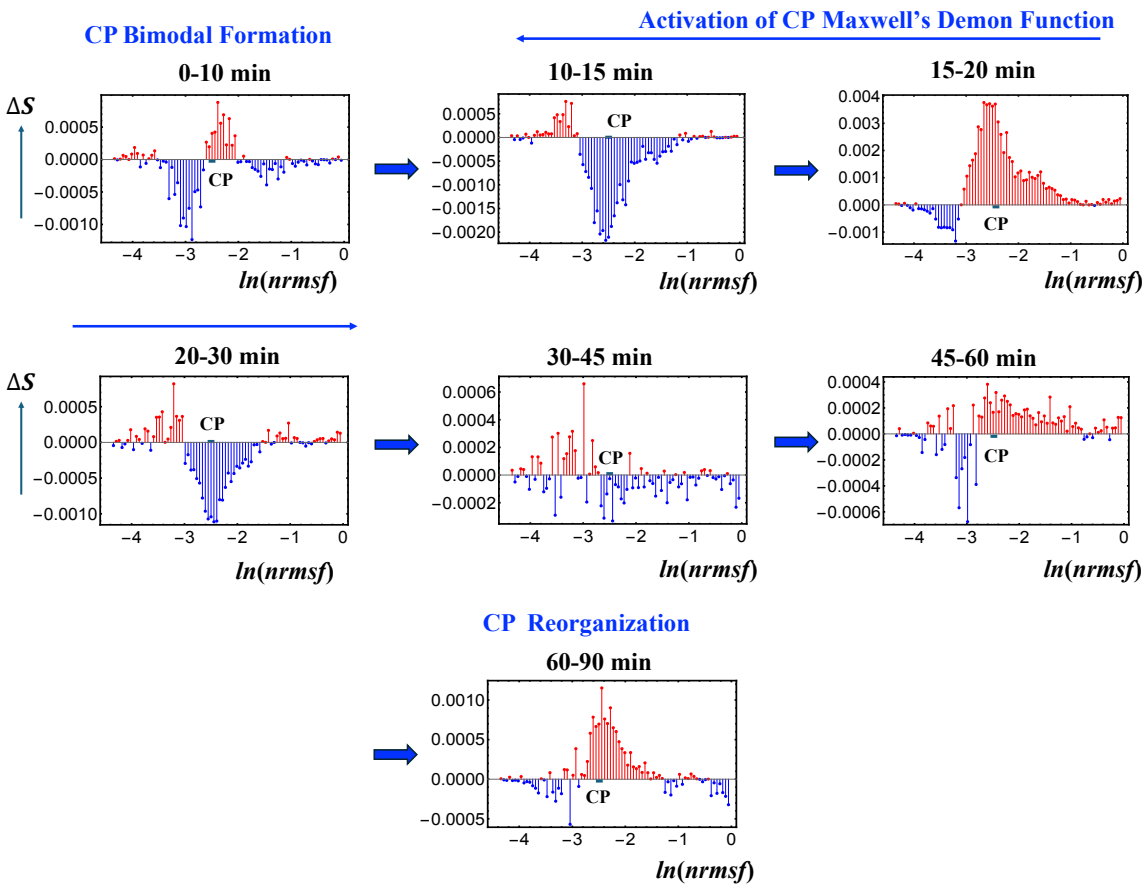

Figure 8: Chromatin Dynamics and CP Formation Across Temporal Entropy Changes

Temporal changes in Shannon entropy associated with chromatin dynamics are plotted against the natural logarithm of *nrmsf* (80 bins) in EGF- **(A)** and HRG-stimulated **(B)** MCF-7 cells. The Critical Point (CP), indicated by the bold black solid line, marks regions where singular bimodal behavior occurs within the range -2.64 < *ln*(*nrmsf*) < -2.52 for EGF stimulation and -2.55 < *ln(nrmsf*) < -2.44 for HRG stimulation (see **Figure 1**). Under EGF stimulation, intermittent CP bimodal patterns emerge at specific intervals (e.g., 0–10 and 20–30 minutes) but repeatedly dissolve without inducing a critical transition or cell fate change.

In contrast, HRG stimulation initially produces a CP bimodal pattern during the 0–10 min period, which transitions into a global coherent fold–unfold chromatin change between 10–30 minutes. This is followed by the re-formation of CP states between 60–90 minutes, aligning with a cell fate transition. These results highlight cyclical chromatin organization states driven by CP–PES phase synchronization and thermodynamic interactions, including Maxwell's demon-like chromatin memory effects.

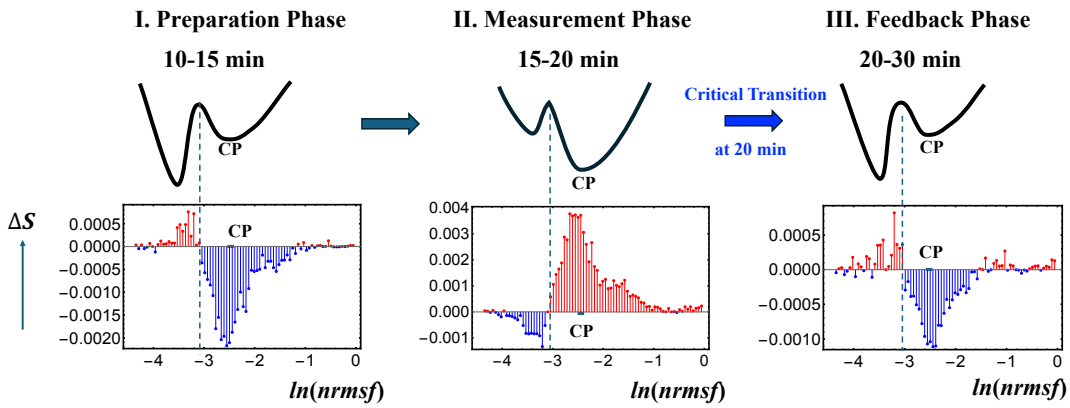

Figure 9: Schematic Representation of a Maxwell's Demon Double-Well Potential Profile. This figure illustrates a conceptual double-well energy landscape representing chromatin dynamics, highlighting the Maxwell's demon-like behavior of the CP (-2.55 < *ln*(*nrmsf*) < -2.44). Each well corresponds to a distinct chromatin state, such as folded or unfolded chromatin, separated by a potential barrier. The vertical axis represents changes in Shannon entropy associated with chromatin remodeling, while the horizontal axis represents the value of *ln*(*nrmsf*) (refer to the main text for details).

3. Discussion: Biophysical Implications

Our findings highlight the genome as an open thermodynamic system operating far from equilibrium. Gene expression and chromatin organization are not static; they are maintained through continuous energy dissipation, allowing cells to adapt flexibly to changing environments. This perspective reveals how biological systems achieve coherence and stability despite external perturbations and how the interplay between chromatin structure and gene regulation can be explained within a dissipative thermodynamic framework.

From a biomedical standpoint, this thermodynamic perspective has substantial implications. By elucidating the principles governing how cells adopt and maintain distinct fates, we gain insights into processes such as cancer progression, metastasis, and therapeutic resistance. Manipulating the genome's regulatory architecture—particularly the "CP," a critical gene set that functions as a central regulatory hub—may offer strategies for reprogramming cell states. For instance, restricting undesirable plasticity in cancer cells or guiding stem cells toward more favorable differentiation pathways could offer new strategies for improved therapeutic interventions.

Autonomous Genome Computing as a Conceptual Framework

Recent advances suggest that genomic DNA is not merely a static blueprint but a dynamic, computationally capable system—a concept we refer to as "genome computing." Here, "computation" describes the genome's autonomous potentiality to integrate diverse regulatory inputs, store adaptive information, and transition between functional states in a context-dependent manner. This perspective offers a unifying framework to understand the nonlinear, adaptive behaviors that regulate gene expression, drive cell differentiation, and govern cellular responses to external cues.

One key insight is that time-dependent transitions in genomic states can be modeled using kinetic equations with cubic nonlinearity, derived from symmetry arguments in thermodynamics. This nonlinearity arises from changes in translational and conformational entropy within large DNA molecules interacting with their associated ionic environments. Experimentally observed chromatin reorganizations support this perspective, suggesting that genomic architecture is continuously tuned to explore and settle into favorable configurations.

The symmetry with cubic nonlinearity mirrors excitability phenomena observed in neuronal systems, as described by the FitzHugh-Nagumo [FitzHugh, 1955; Nagumo et al., 1962] and Hodgkin-Huxley [Hodgkin and Huxley, 1952] frameworks. While these parallels remain conceptual, they underscore a shared principle: nonlinear systems, whether neural or genomic, can exhibit threshold-dependent switching between stable states.

Recent evidence clearly demonstrates that genome-sized DNA exhibits a bimodal free energy profile [Yoshikawa et al., 2000; Iwaki et al., 2003; Nakai et al., 2005; Mayama et al., 2007; Estévez-Torres et al., 2011; Yoshikawa et al., 2011; Nishio et al., 2020]. This bimodal symmetry inherently implies cubic nonlinearity in the reaction kinetics, which arises from the functional derivative of the free energy [Yoshikawa, 2002；Takenaka et al., 2008: Nagahara and Yoshikawa, 2010; Kanemura et al., 2018].

At the heart of these transitions lies the occurrence of the Critical Point (CP). While its precise composition remains to be fully delineated, existing evidence suppots that specific genomic regions consistently orchestrate large-scale regulatory shifts. As cells approach critical decision

points—such as lineage commitment—the CP emerges from bimodal states, toggling chromatin configurations between more and less active forms. Observations of pericentromere-associated domain (PAD) rearrangements and chromatin remodeling [Krigerts et al., 2021] further support the notion that the CP governs these critical transitions, effectively "choosing" among distinct genomic states.

These transitions can be conceptualized through an energy landscape perspective, where changes in translational and conformational entropy reshape the free energy landscape, favoring certain pathways over others. Analogies with Ginzburg-Landau theory [Ginzburg and Landau, 1965] highlight the importance of identifying order parameters (e.g., chromatin compaction or gene network states) and recognizing that critical transitions occur when specific thresholds are crossed. Our self-organized criticality (SOC) provides another useful framework: the genome, via the CP, naturally tunes itself to critical points, maintaining a balance between order and flexibility. Acting as rewritable chromatin memory, the CP plays a role akin to Maxwell's demon, selectively promoting transitions that reduce uncertainty and drive the system toward coherent and functionally relevant states.

This notion of "genome computing" does not imply that the genome functions like a digital processor with discrete inputs and outputs. Instead, genome computing is characterized by autonomous, decentralized super-information processing. It reflects a continuous, adaptive reshaping of genomic states, where "memory" is encoded in the genome's ability to revisit specific conformations, and "logic" emerges from network interactions that drive transitions toward or away from stable regulatory configurations.

In conjunction with the genomic-thermodynamic mechanism, understanding how the CP functions as a central process hub to orchestrate the complex spatiotemporal self-organization of the genome will elucidate fundamental principles governing cell fate, development, and stress responses. This knowledge should ultimately inspire innovative approaches in regenerative medicine, cancer therapy, and synthetic biology.

Genome Intelligence (GI) Supported by Autonomous Genome Computing

On a more theoretical level, the concept of GI builds upon the computational principles of genome computing to describe the genome's ability to exhibit integrated, adaptive, and memory-like behavior. Here, intelligence refers to a minimal form of integrated responsiveness, where the genome does not merely react to environmental stimuli but incorporates these stimuli into its regulatory framework, enabling adaptation and future decision-making.

Integrated Information Theory (IIT), initially developed to explain consciousness in neural systems, provides a useful framework for understanding intelligence in biological systems. The fundamental challenge of IIT lies in the integration of external informative stimuli into the structure of the 'intelligent agent,' leading to the emergence of a 'memory' of the stimulus. This stands in contrast to non-intelligent sensors (e.g., a photodiode), whose structure remains unchanged by their interaction with the sensed stimulus.

As demonstrated by Niizato et al. [Niizato et al., 2024], IIT extends beyond neural systems to describe integrated information within molecular and cellular systems, where complex interactions produce irreducible wholes. Applying this principle to the genome, GI arises from the integration of external signals into chromatin configurations, regulatory networks, and gene expression states. This capacity for integration, persistence, and reconfiguration distinguishes the genome as an autonomous intelligent system.

While genome computing describes the mechanisms by which the genome processes and integrates information, GI emphasizes the emergent properties of this system. Intelligence reflects the genome's ability to actively discriminate between different environmental or internal states, enabling a nuanced understanding of the cellular context. By integrating these states into its chromatin structure and regulatory networks, the genome establishes a foundation for dynamic memory, encoding past experiences to inform future actions. Furthermore, this intelligence allows the genome to adaptively guide transitions to future regulatory configurations, ensuring cellular responses remain both coherent and flexible in the face of changing conditions.

This mechanism corresponds to the emergence of a set of strongly correlated subsets of genes, as described by Dynamic Network Biomarker (DNB) theory [Aihara et al., 2022]. DNB theory

highlights how such subsets act as early indicators of critical transitions, emphasizing the coordination of gene dynamics during these pivotal moments. Additionally, this behavior is tied to an increase in the power of a minor principal component orthogonal to the "tissue attractor" main principal component, as shown by Zimatore et al. [Zimatore et al., 2021]. These findings underline the genomic system's ability to consolidate information across scales, creating a dynamic regulatory network that integrates both structural and functional changes.

For example, in supercritical states, the genome demonstrates a heightened sensitivity to perturbations, enabling rapid transitions that propagate across the chromatin landscape. These transitions are not random but are orchestrated by the OMG (oscillatory mode genes)–CP–GA (critical point–genome attractor) network [Tsuchiya et al., 2023a], which align the genome's response with the needs of the cell. Such behavior mirrors the minimal criteria for intelligence outlined in IIT, where integrated information is both created and used to maintain system coherence.

In principle, genome-based systems could be engineered to construct dynamic logical networks, such as non-binary finite state machines [Yeo et al., 2007; Moon et al., 2012; Doe and Smith, 2023]. These systems replicate genome intelligence in synthetic or computational contexts by mimicking critical-state hubs, such as the OMG–CP–GA network. These hubs reflect the genome's inherent capacity for adaptation and self-organization. As noted by Zimatore et al. [Zimatore et al. 2021], subsets of genes driving these transitions are enriched in chromatin-folding dynamics, reinforcing the idea that genomic intelligence emerges from its ability to orchestrate large-scale structural and regulatory changes.

Ultimately, GI reframes our understanding of the genome as a dynamic, adaptive, and integrative system. By uniting computational and thermodynamic principles with biological mechanisms, this concept provides a foundation for exploring how genomes encode past experiences, adapt to changing conditions, and guide cellular behavior. This perspective has profound implications for fields ranging from regenerative medicine to synthetic biology, where leveraging the intelligent properties of the genome could revolutionize how we design and manipulate living systems.

4. Conclusion

Our study demonstrates that genomic regulation can be understood through the lens of open stochastic thermodynamics. Rather than existing at thermodynamic equilibrium, gene expression operates far from equilibrium, with continuous energy dissipation enabling dynamic regulation, adaptability, and responsiveness to external cues. By examining the roles of critical point (CP) genes and the whole expression system (WES) in MCF-7 breast cancer cells, we present a thermodynamic framework that explains how biological systems autonomously maintain coherence, stability, and flexibility in their gene expression profiles.

Key insights from our findings include the thermodynamic phase synchronization of CP genes with the genome, the distinct roles of the CP under different stimuli, and the presence of negative high-order mutual information, which highlights synergistic, non-pairwise interactions among genes. For example, under epidermal growth factor (EGF) stimulation, the CP remains passive, preserving stability without transitioning into a new state. In contrast, under heregulin (HRG) stimulation, the CP operates like a "Maxwell's demon," orchestrating entropic and informational dynamics to "rewrite" chromatin, encode past cellular states, and drive critical cell fate changes.

On a broader level, these computational dynamics support the concept of GI, where the genome exhibits emergent properties such as the ability to discriminate between environmental states, integrate signals into its structural framework, and adaptively guide future regulatory transitions. This emergent intelligence reflects the genome's capacity to store "memory" of past states and utilize this information to navigate complex decision-making landscapes. These insights bridge classical molecular genetics with nonequilibrium thermodynamic and computational principles, providing a holistic view of genome regulation.

Our findings open new avenues for understanding disease progression, guiding regenerative medicine, and informing innovative cancer therapies. For example, the CP's ability to dynamically "compute" and integrate signals highlights opportunities for targeting critical regulatory hubs in cancer treatment or leveraging genomic intelligence in synthetic biology to design adaptive, programmable cellular systems.

From a global perspective, this integration of genome computing and intelligence inspires the development of machine learning tools modeled on cell fate transition dynamics. Physics-Informed Neural Networks (PINNs), as described by Cai et al. [Cai et al., 2021], offer a promising

framework for incorporating physical principles into neural network architectures to replicate the behavior of biological systems. Similarly, Hopfield networks, as noted by Krotov [Krotov, 2023], demonstrate how network correlations can encode emergent behavior, much like genomic systems encode adaptive regulatory transitions. By applying these computational principles as hyper-parallel autonomous decentralized systems, we can enhance both biological understanding and machine learning, paving the way for models that seamlessly integrate thermodynamic, computational, and biological insights.

5. Material

Microarray data for the activation of ErbB receptor ligands in human breast cancer MCF-7 cells by EGF and HRG; Gene Expression Omnibus (GEO) ID: GSE13009 (N = 22277 mRNAs; for experimental details see [Saeki et al., 2009]) at 18 time points: $t_1 = 0$, $t_2 = 10$, 15, 20, 30, 45, 60, 90 min, 2, 3, 4, 6, 8, 12, 24, 36, 48, $t_T = 18 = 72$h. The robust multichip average (RMA) was used to normalize expression data for further background adjustment and to reduce false positives [Bolstad et al., 2003; Irizarry et al., 2003; McClintick and Edenberg, 2006].

6. Apenndix: Mathematical description of Chromatin Entropy

As illustrated in **Figure 7**, we transformed the expression distribution into the normalized root mean square fluctuation (*nrmsf*) probability distribution—an entropy decomposition approach analogous to the logical/physical state framework described by Maroney [Maroney, 2009]. To provide a mathematical perspective, we describe chromatin entropy by showing how the Shannon entropy of the Whole Expression System (WES), defined in equation (2), into "logical states" corresponding to *nrmsf* bins as follows:

$$S\left(X(t_j)\right) = -\sum_i P\left(x_i(t_j)\right) ln\left(P\left(x_i(t_j)\right)\right)$$

$$= -\sum_m \sum_{x_i \in m} P(x_i(t_j)|m) \cdot P(m) \cdot ln\left(P(x_i(t_j)|m) \cdot P(m)\right)$$

$$= -\sum_{m}\sum_{x_i \in m} P\big(x_i(t_j)\big|m\big) \cdot P(m) \cdot \Big(ln\Big(P\big(x_i(t_j)\big|m\big)\Big) + ln\big(P(m)\big)\Big)$$

$$= \quad S(M) + \ \sum_m P(m) \cdot S\Big(Y_m(t_j)\Big). \tag{16}$$

Here, the probability $P(x_i(t_j))$ of gene x_i being expressed at time t_j can be factored into 1) the probability of selecting a logical state m, $P(m)$, and 2) the probability of the physical state $x_i(t_j)$ within that logical state, $P(x_i(t_j)|m)$, such that $P(x_i(t_j)) = P(x_i(t_j)|m) \cdot P(m)$. The sum of probabilities within each logical state satisfies $\sum_{x_i} P\big(x_i(t_j)\big|m\big) = 1$ at time t_j.

The entropy of the whole expression system, S(WES), is thus expanded in terms of $S(M)$, the entropy associated with the distribution of logical states, and $S(Y_m(t_j))$, which represents the entropy of the physical states (gene expression levels) within the mth logical state:

$$S(M) = -\sum_m P(m) \cdot ln\big(P(m)\big), \tag{17}$$

and

$$S\Big(Y_m(t_j)\Big) = -\sum_{x_i \in m} P(x_i(t_j)|m) \cdot ln\big(P(x_i(t_j)|m)\big). \tag{18}$$

Author Contribution

MT: Conceptualization (Lead); Formal Analysis and Software; Methodology; Writing – Original Draft; Writing – Review & Editing

KY: Conceptualization (Supporting); Writing – Review & Editing

AG: Conceptualization (Supporting); Writing – Review & Editing

Acknowledgments

MT thanks Prof. Paul Brazhnik for his insightful discussions and the SEIKO Life Science Laboratory, Osaka, Japan, for its invaluable support during this research. He is also grateful to his family—Ms. Takako Tsuchiya, Drs. Kimiko & Kazumi Tsuchiya, and Dr. Harry Taylor—for their

constant encouragement. Special thanks go to Dr. Dasaku Ikeda for his lifelong inspiration and to Ms. Satoko Takeda & Ms. Hisami Spector jfor their kind and heartfelt support.

References

Adami, C. (2004). Information theory in molecular biology. Phys. Life Rev., 1, 3–22. https://doi.org/10.1016/j.plrev.2004.01.002

Aihara, K., Liu, R., Koizumi, K., Liu, X., & Chen, L. (2022). Dynamical network biomarkers: Theory and applications. Gene, 808, 145997. https://doi.org/10.1016/j.gene.2021.145997

Annby-Andersson, B., Bhattacharyya, D., Bakhshinezhad, P., Holst, D., De Sousa, G., Jarzynski, C., Samuelsson, P., & Potts, P. P. (2024). Maxwell's demon across the quantum-to-classical transition. Phys. Rev. Res., 6, 043216. https://doi.org/10.1103/PhysRevResearch.6.043216

Bak, P., Tang, C., & Wiesenfeld, K. (1987). Self-organized criticality: An explanation of the 1/f noise. Phys. Rev. Lett., 59, 381–384. https://doi.org/10.1103/PhysRevLett.59.381

Bak, P., Tang, C., & Wiesenfeld, K. (1988). Self-organized criticality. Phys. Rev. A, 38, 364–374. https://doi.org/10.1103/PhysRevA.38.364

Bak, P., & Chen, K. (1991). Self-organized criticality. Sci. Am., 264, 46–53.

Barato, A. C., & Seifert, U. (2014). Unifying three perspectives on information processing in stochastic thermodynamics. Phys. Rev. Lett., 112, 090601. https://doi.org/10.1103/PhysRevLett.112.090601

Bennett, C. H. (2003). Notes on Landauer's principle, reversible computation, and Maxwell's demon. Stud. Hist. Philos. Mod. Phys., 34, 501–510. https://doi.org/10.1016/S1355-2198(03)00039-X

Bérut, A., Arakelyan, A., Petrosyan, A., Ciliberto, S., Dillenschneider, R., & Lutz, E. (2012). Experimental verification of Landauer’s principle linking information and thermodynamics. Nature, 483, 187–189. https://doi.org/10.1038/nature10872

Bolstad, B. M., Irizarry, R. A., Åstrand, M., & Speed, T. P. (2003). A comparison of normalization methods for high density oligonucleotide array data based on variance and bias. Bioinformatics, 19, 185–193. https://doi.org/10.1093/bioinformatics/19.2.185

Cai, S., Wang, Z., Fuest, F., Jeon, Y. J., Gray, C., & Karniadakis, G. E. (2021). Flow over an espresso cup: Inferring 3-D velocity and pressure fields from tomographic background oriented

Schlieren via physics-informed neural networks. J. Fluid Mech., 915, A102. https://doi.org/10.1017/jfm.2021.135

Censi, F., Giuliani, A., Bartolini, P., & Calcagnini, G. (2011). A multiscale graph theoretical approach to gene regulation networks: A case study in atrial fibrillation. IEEE Trans. Biomed. Eng., 58, 2943–2946. https://doi.org/10.1109/TBME.2011.2150747

Ciofani, M., Madar, A., Galan, C., Sellars, M., Mace, K., Pauli, F., Agarwal, A., Huang, W., Parkhurst, C. N., Muratet, M., Newberry, K. M., Meadows, S., Greenfield, A., Yang, Y., Jain, P., Kirigin, F. K., Birchmeier, C., Wagner, E. F., Murphy, K. M., Myers, R. M., Bonneau, R., & Littman, D. R. (2012). A validated regulatory network for Th17 cell specification. Cell, 151, 289–303. https://doi.org/10.1016/j.cell.2012.09.016

Deng, Q., Ramsköld, D., Reinius, B., & Sandberg, R. (2014). Single-cell RNA-seq reveals dynamic, random monoallelic gene expression in mammalian cells. Science, 343, 193–196. https://doi.org/10.1126/science.1245316

Doe, J., & Smith, J. (2023). Modeling gene regulatory networks with non-binary finite state machines: A synthetic biology approach. J. Theor. Biol., 456, 123–145. https://doi.org/10.1016/j.jtbi.2023.123456

Flatt, S., Busiello, D. M., Zamuner, S., & De Los Rios, P. (2023). ABC transporters are billion-year-old Maxwell Demons. Commun. Phys., 6, 205. https://doi.org/10.1038/s42005-023-01320-y

FitzHugh, R. (1955). Mathematical models of threshold phenomena in the nerve membrane. Bull. Math. Biophys., 17, 257–278.

Ginzburg, V. L., & Landau, L. D. (1950). On the theory of superconductivity. Zh. Eksp. Teor. Fiz., 20, 1064–1082.

Giuliani, A., Tsuchiya, M., & Yoshikawa, K. (2017). Self-organization of genome expression from embryo to terminal cell fate: Single-cell statistical mechanics of biological regulation. Entropy, 20, 13. https://doi.org/10.3390/e20010013

Hodgkin, A. L., & Huxley, A. F. (1952). A quantitative description of membrane current and its application to conduction and excitation in nerve. J. Physiol., 117, 500–544. https://doi.org/10.1113/jphysiol.1952.sp004764

Hu, K. T. (1962). On the amount of information. Theory Probab. Appl., 7, 439–447.
Huang, S., Eichler, G., Bar-Yam, Y., & Ingber, D. E. (2005). Cell fates as high-dimensional attractor states of a complex gene regulatory network. Phys. Rev. Lett., 94, 128701. https://doi.org/10.1103/PhysRevLett.94.128701

Hübner, K., & Szekely, G. (2010). Information theoretical estimation of the complexity of neural codes. Phys. Rev. E, 81, 011914. https://doi.org/10.1103/PhysRevE.81.011914

Irizarry, R. A., Hobbs, B., Collin, F., Beazer-Barclay, Y. D., Antonellis, K. J., Scherf, U., & Speed, T. P. (2003). Exploration, normalization, and summaries of high density oligonucleotide array probe level data. Biostatistics, 4, 249–264. https://doi.org/10.1093/biostatistics/4.2.249

Iwaki, T., & Yoshikawa, K. (2003). Competition between interchain and intrachain phase segregation. Phys. Rev. E, 68, 031902. https://doi.org/10.1103/PhysRevE.68.031902
Ito, S. (2018). Stochastic thermodynamic interpretation of information geometry. Phys. Rev. Lett., 121, 030605. https://doi.org/10.1103/PhysRevLett.121.030605

Kanemura, A., Yoshikawa, Y., Fukuda, W., Tsumoto, K., Kenmotsu, T., & Yoshikawa, K. (2018). Opposite effect of polyamines on in vitro gene expression: Enhancement at low concentrations but inhibition at high concentrations. PLoS ONE, 13, e0193595.

Korbel, J., & Wolpert, D. H. (2024). Nonequilibrium thermodynamics of uncertain stochastic processes. Phys. Rev. Res., 6, 013021. https://doi.org/10.1103/PhysRevResearch.6.013021

Krigerts, J., Salmina, K., Freivalds, T., Zayakin, P., Rumnieks, F., Inashkina, I., Giuliani, A., Hausmann, M., & Erenpreisa, J. (2021). Differentiating cancer cells reveal early large-scale genome regulation by pericentric domains. Biophys. J., 120, 711–724. https://doi.org/10.1016/j.bpj.2021.01.002

Krotov, D. (2023). A new frontier for Hopfield networks. Nat. Rev. Phys., 5, 295–307. https://doi.org/10.1038/s42254-023-00595-y

Landauer, R. (1961). Irreversibility and heat generation in the computing process. IBM J. Res. Dev., 5, 183–191. https://doi.org/10.1147/rd.53.0183

Liu, X., Chang, X., Liu, R., Yu, X., Chen, L., & Aihara, K. (2017). Quantifying critical states of complex diseases using single-sample dynamic network biomarkers. PLoS Comput. Biol., 13, e1005633.

Maroney, O. J. E. (2009). Generalizing Landauer's principle. Phys. Rev. E, 79, 031105. https://doi.org/10.1103/PhysRevE.79.031105

Maxwell, J. C. (1871). Theory of Heat. Longmans, Green, and Co.

Mayama, H., Nakai, T., Takushi, E., Tsujii, K., & Yoshikawa, K. (2007). Marked differences in volume phase transitions between gel and single molecule in DNA. J. Chem. Phys., 127, 034901. https://doi.org/10.1063/1.2748767

McClintick, J. N., & Edenberg, H. J. (2006). Effects of filtering by present call on analysis of microarray experiments. BMC Bioinformatics, 7, 49. https://doi.org/10.1186/1471-2105-7-49

McGill, W. J. (1954). Multivariate information transmission. Psychometrika, 19, 97–116. https://doi.org/10.1007/BF02289159

Moon, T. S., Lou, C., Tamsir, A., Stanton, B. C., & Voigt, C. A. (2012). Genetic programs constructed from layered logic gates in single cells. Nature, 491, 249–253. https://doi.org/10.1038/nature11516

Nagahara, H., & Yoshikawa, K. (2010). Large system in a small cell: A hypothetical pathway from a microscopic stochastic process towards robust genetic regulation. Chem. Phys. Lett., 494, 88–94. https://doi.org/10.1016/j.cplett.2010.05.042

Nagashima, T., Shimodaira, H., Ide, K., Nakakuki, T., Tani, Y., Takahashi, K., Yumoto, N., & Hatakeyama, M. (2007). Quantitative transcriptional control of ErbB receptor signaling undergoes graded to biphasic response for cell differentiation. Journal of Biological Chemistry, 282(6), 4045–4056. https://doi.org/10.1074/jbc.M608653200

Nagumo, J., Arimoto, S., & Yoshizawa, S. (1962). An active pulse transmission line simulating nerve axon. Proc. IRE, 50, 2061–2070. https://doi.org/10.1109/JRPROC.1962.288235

Nakai, T., Hizume, K., Yoshimura, S. H., Takeyasu, K., & Yoshikawa, K. (2005). Phase transition in reconstituted chromatin. Europhys. Lett., 69, 1024–1030. https://doi.org/10.1209/epl/i2004-10460-7

Niizato, T., Sakamoto, K., Mototake, Y., Murakami, H., & Tomaru, T. (2024). Information structure of heterogeneous criticality in a fish school. Sci. Rep., 14, 29758. https://doi.org/10.1038/s41598-024-79232-2

Parrondo, J. M. R., Horowitz, J. M., & Sagawa, T. (2015). Thermodynamics of information. Nat. Phys., 11, 131–139. https://doi.org/10.1038/nphys3230

Peliti, L., & Pigolotti, S. (2021). Stochastic Thermodynamics: An Introduction. Princeton University Press.

Rosas, F. E., Mediano, P. A. M., Gastpar, M., & Jensen, H. J. (2019). Quantifying high-order interdependencies via multivariate extensions of the mutual information. Phys. Rev. E, 100, 032305. https://doi.org/10.1103/PhysRevE.100.032305

Saeki, Y., Endo, T., Ide, K., Nagashima, T., Yumoto, N., Toyoda, T., Suzuki, H., Hayashizaki, Y., Sakaki, Y., & Okada-Hatakeyama, M. (2009). Ligand-specific sequential regulation of transcription factors for differentiation of MCF-7 cells. BMC Genomics, 10, 545. https://doi.org/10.1186/1471-2164-10-545

Sagawa, T., & Ueda, M. (2012a). Nonequilibrium thermodynamics of feedback control. Phys. Rev. E, 85, 021104. https://doi.org/10.1103/PhysRevE.85.021104

Sagawa, T., & Ueda, M. (2012b). Fluctuation theorem with information exchange: Role of correlations in stochastic thermodynamics. Phys. Rev. Lett., 109, 180602. https://doi.org/10.1103/PhysRevLett.109.180602

Seifert, U. (2012). Stochastic thermodynamics, fluctuation theorems, and molecular machines. Rep. Prog. Phys., 75, 126001. https://doi.org/10.1088/0034-4885/75/12/126001

Shannon, C. E. (1948). A mathematical theory of communication. Bell Syst. Tech. J., 27, 379–423, 623–656. https://doi.org/10.1002/j.1538-7305.1948.tb01338.x

Shiraishi, N. (2023). An Introduction to Stochastic Thermodynamics: From Basic to Advanced. Springer, Singapore.
Shmulevich, I., Kauffman, S. A., & Aldana, M. (2005). Eukaryotic cells are dynamically ordered or critical but not chaotic. Proc. Natl. Acad. Sci. U.S.A., 102, 13439–13444. https://doi.org/10.1073/pnas.0506771102

Szilard, L. (1929). Über die Entropieverminderung in einem thermodynamischen System bei Eingriffen intelligenter Wesen. Z. Phys., 53, 840–856. https://doi.org/10.1007/BF01341281

Takenaka, Y., Nagahara, H., Kitahata, H., & Yoshikawa, K. (2008). Large-scale on-off switching of genetic activity mediated by the folding-unfolding transition in a giant DNA molecule: A hypothesis. Phys. Rev. E, 77, 031905. https://doi.org/10.1103/PhysRevE.77.031905

Timme, N., Alford, W., Flecker, B., & Beggs, J. M. (2014). Synergy, redundancy, and multivariate information measures: an experimentalist's perspective. J. Comput. Neurosci., 36, 119–140. https://doi.org/10.1007/s10827-013-0458-4

Estévez-Torres, A., & Baigl, D. (2011). DNA compaction: fundamentals and applications. Soft Matter, 7, 6746–6756. https://doi.org/10.1039/C1SM05373F

Toyabe, S., Sagawa, T., Ueda, M., Muneyuki, E., & Sano, M. (2010). Experimental demonstration of information-to-energy conversion and validation of Szilard's engine. Nat. Phys., 6, 988–992. https://doi.org/10.1038/nphys1821

Tsuchiya, M., Piras, V., Giuliani, A., Tomita, M., & Selvarajoo, K. (2010). Collective dynamics of specific gene ensembles crucial for neutrophil differentiation: The existence of genome vehicles revealed. PLoS ONE, 5, e12116. https://doi.org/10.1371/journal.pone.0012116

Tsuchiya, M., Hashimoto, M., Takenaka, Y., Motoike, I. N., & Yoshikawa, K. (2014). Global genetic response in a cancer cell: Self-organized coherent expression dynamics. PLoS ONE, 9, e97411. https://doi.org/10.1371/journal.pone.0097411

Tsuchiya, M., Giuliani, A., Hashimoto, M., Erenpreisa, J., & Yoshikawa, K. (2015). Emergent self-organized criticality in gene expression dynamics: Temporal development of global phase transition revealed in a cancer cell line. PLoS ONE, 10, e0128565. https://doi.org/10.1371/journal.pone.0128565

Tsuchiya, M., Giuliani, A., Hashimoto, M., Erenpreisa, J., & Yoshikawa, K. (2016). Self-organizing global gene expression regulated through criticality: Mechanism of the cell-fate change. PLoS ONE, 11, e0167912. https://doi.org/10.1371/journal.pone.0167912

Tsuchiya, M., Giuliani, A., & Yoshikawa, K. (2020). Cell-fate determination from embryo to cancer development: Genomic mechanism elucidated. Int. J. Mol. Sci., 21, 4581–4617. https://doi.org/10.3390/ijms21134581

Tsuchiya, M., Giuliani, A., Zimatore, G., Erenpreisa, J., & Yoshikawa, K. (2022). A unified genomic mechanism of cell-fate change. Results Probl. Cell Differ., 70, 35–69. https://doi.org/10.1007/978-3-031-06573-6_2

Tsuchiya, M., Brazhnik, P., Bizzarri, M., & Giuliani, A. (2023a). Synchronization between attractors: Genomic mechanism of cell-fate change. Int. J. Mol. Sci., 24, 11603. https://doi.org/10.3390/ijms241411603

Tsuchiya, M., Giuliani, A., & Brazhnik, P. (2023b). From cell states to cell fates: Control of cell state transitions. Methods Mol. Biol., 2745, 137–162. https://doi.org/10.1007/978-1-0716-3577-3_9

Watkins, N. W., Pruessner, G., Chapman, S. C., Crosby, N. B., & Jensen, H. J. (2016). 25 years of self-organized criticality: Concepts and controversies. Space Science Reviews, 198(1-4), 3–44. https://doi.org/10.1007/s11214-015-0155-x

Yang, C. X., Liu, Z., Fleurot, R., Adenot, P., Duranthon, V., Vignon, X., Zhou, Q., Renard, J. P., & Beaujean, N. (2013). Heterochromatin reprogramming in rabbit embryos after fertilization, intra-, and inter-species SCNT correlates with preimplantation development. Reproduction, 145, 149–159. https://doi.org/10.1530/REP-11-0421

Yeo, Z. X., Wong, S. T., Arjunan, S. N. V., Piras, V., Tomita, M., Selvarajoo, K., Giuliani, A., & Tsuchiya, M. (2007). Sequential logic model deciphers dynamic transcriptional control of gene expressions. PLoS ONE, 2, e776. https://doi.org/10.1371/journal.pone.0000776

Yoshikawa, K. (2002). Field hypothesis on the self-regulation of gene expression. J. Biol. Phys., 28, 701–712. https://doi.org/10.1023/A:1021251125101

Yoshikawa, Y., Nomura, S. M., Kanbe, T., & Yoshikawa, K. (2000). Controlling the folding/unfolding transition of the DNA–histone H1 complex by direct optical manipulation. Chem. Phys. Lett., 330, 77–82. https://doi.org/10.1016/S0009-2614(00)01075-7

Yoshikawa, Y., Suzuki, Y., Yamada, K., Fukuda, W., Yoshikawa, K., Takeyasu, K., & Imanaka, T. (2011). Critical behavior of megabase-size DNA toward the transition into a compact state. J. Chem. Phys., 135, 225101. https://doi.org/10.1063/1.3666845

Zimatore, G., Tsuchiya, M., Hashimoto, M., Kasperski, A., & Giuliani, A. (2021). Self-organization of whole-gene expression through coordinated chromatin structural transition. Biophys. Rev., 2, 031303. https://doi.org/10.1063/5.0058511